Deep–Sea Research I 164 (2020) 103322

Contents lists available at ScienceDirect

Deep-Sea Research Part I

journal homepage: http://www.elsevier.com/locate/dsri

Spanning the depths or depth-restricted: Three new species of *Bathymodiolus* (Bivalvia, Mytilidae) and a new record for the hydrothermal vent *Bathymodiolus thermophilus* at methane seeps along the Costa Rica margin

Marina F. McCowin *, Caitlin Feehery, Greg W. Rouse **

Scripps Institution of Oceanography, University of California San Diego, La Jolla, CA, 92093-0202, USA

ARTICLE INFO

Keywords:
Bathymodiolinae
Cold seeps
New species
East pacific

ABSTRACT

Bathymodiolus Kenk and Wilson, 1985 includes fourteen currently recognized species from deep-sea chemosynthetic environments in the Pacific, Atlantic, and Indian oceans. In this study, phylogenetic analyses of mytilid mussels sampled from seeps along the Costa Rica margin reveal the presence of three new *Bathymodiolus* species, sampled from depths across ~1000–1900 m. *Bathymodiolus billschneideri* n. sp., *B. earlougheri* n. sp., and *B. nancyschneiderae* n. sp. differ genetically from congeneric species of *Bathymodiolus* and show some stratification by depth. The depth ranges of *Bathymodiolus billschneideri* n. sp., *B. nancyschneiderae* n. sp., and *B. earlougheri* n. sp. were ~1400–1900 m, 1000–1100 m, and ~1000–1900m, respectively. *Bathymodiolus billschneideri* n. sp. and *B. earlougheri* n. sp. were found to be closely related to *Bathymodiolus thermophilus* Kenk and Wilson, 1985, while *B. nancyschneiderae* n. sp. exhibited closer relationships to non-East-Pacific taxa. *Bathymodiolus thermophilus* was the first *Bathymodiolus* mussel discovered, sampled from a vent along the Galápagos Rift Zone in 1985 and later recorded along much of the East Pacific Rise. This study confirms the presence of *B. thermophilus* at the Costa Rica margin, representing the first DNA and morphological samples of *B. thermophilus* at a seep environment. Analysis of habitat evolution suggests that *B. thermophilus* and its closest relative, *B. antarcticus* Johnson and Vrijenhoek, 2013, are of seep ancestry.

1. Introduction

Bathymodiolinae Kenk and Wilson, 1985 is a subfamily of the Mytilidae mussel group whose members inhabit reducing environments worldwide (Kiel, 2010; Taylor and Glover, 2010). Within Bathymodiolinae, the eight currently accepted genera contain over fifty named species (Kenk and Wilson, 1985; Olu-Le Roy et al., 2007; Taylor and Glover, 2010): *Adipicola* Dautzenberg, 1927, *Bathymodiolus* Kenk and Wilson, 1985, *Benthomodiolus* Dell, 1987, *Gigantidas* Cosel and Marshall, 2003, *Idas* Jeffreys, 1876, *Tamu* Gustafson, Turner, Lutz & Vrijenhoek, 1998, *Terua* Dall, Bartsch and Rehder, 1938 and *Vulcanidas* Cosel and Marshall, 2010. Many of these mussels, such as *Bathymodiolus*, are chemosymbiotic, relying on sulphide and/or methane-oxidizing symbionts in the ctenidia for much of their nutritional requirements (Fisher et al., 1993; Duperron et al., 2008; Taylor and Glover, 2010). *Bathymodiolus* are restricted to deep-sea chemosynthetic environments such as vents and seeps, where they often serve as foundational species and dominate the community biomass, creating essential habitat space for other organisms (Govenar, 2010; Vrijenhoek, 2010; Xu et al., 2019). *Bathymodiolus* currently includes 14 accepted species, distributed in the Atlantic, Pacific, and Indian oceans, as well as the Caribbean and Gulf of Mexico (Cosel et al., 1999; Cosel and Olu, 1998; Gustafson et al., 1998; Hashimoto, 2001). However, molecular data suggests that *Bathymodiolus* is not monophyletic (Cosel and Marshall, 2003; Jones et al., 2006; Lorion et al., 2010).

Historically, Bathymodiolinae species were described based on morphological characteristics such as shell dimensions and internal anatomy (Kenk and Wilson, 1985), but molecular data has greatly changed the understanding of the group's internal relationships. For example, DNA sequence data suggested that both *Bathymodiolus* and

* Corresponding author.
** Corresponding author.
E-mail addresses: marruda@ucsd.edu (M.F. McCowin), grouse@ucsd.edu (G.W. Rouse).

https://doi.org/10.1016/j.dsr.2020.103322
Received 29 January 2020; Received in revised form 7 May 2020; Accepted 19 May 2020
Available online 16 July 2020

Gigantidas were paraphyletic or polyphyletic (Jones et al., 2006). The paraphyly of *Gigantidas* has been recently resolved (see summary in Xu et al., 2019), while the paraphyly of *Bathymodiolus* has yet to be remedied. *Bathymodiolus manusensis* Hashimoto and Furuta, 2007 and *B. aduloides* Hashimoto and Okutani, 1994 are clearly not members of the *Bathymodiolus* clade containing the type species for the genus, so we have placed their names in quotation marks, echoing the treatment by Gustafson et al. (1998), to indicate the nomenclatural problems regarding these taxa. While the taxonomy of *Bathymodiolus* needs some revision, new species of Bathymodiolinae are still being described (e.g. *Gigantidas haimaensis* Xu et al., 2019).

This study focuses on mussels collected from deep-sea seeps at various depths along the Costa Rica margin in the eastern Pacific Ocean (Fig. 1). These collections include unidentified *Bathymodiolus* and *B. thermophilus* Kenk and Wilson, 1985 specimens that had been noted previously at these seeps (Levin et al., 2012, 2015). The Costa Rica margin in the East Pacific represents a biodiverse and variable seep habitat for many chemosymbiotic fauna, with over 40 seeps discovered along the margin since 2008 (Sahling et al., 2008; Levin et al., 2012, 2015). *Bathymodiolus thermophilus* is well-known from hydrothermal vents along the East Pacific Rise, but had not been previously sampled outside of the East Pacific Rise or Galápagos Rift, or at any seep environments, until it was observed at the Jaco Scar seep (which exhibits some vent-like characteristics) on the Costa Rica margin (Levin et al., 2012). Here we combine newly generated DNA data for *Bathymodiolus* mussels sampled from five seep sites in Costa Rica (999–1891 m) with previously published DNA data (Table 1) to substantiate the presence of *B. thermophilus* (as reported in Levin et al., 2012) and reveal three new species of *Bathymodiolus* at seeps along the Costa Rica margin, which are described here.

2. Methods

2.1. Sampling

Bathymodiolus mussels were collected and subsampled for DNA on several dives by the HOV *Alvin* and ROV *SuBastian* between 2009 and 2019 along the Costa Rica margin at the following dive sites between 999 and 1891 m: Mound 12, Jaco-1000, The Thumb, Parrita Seep (formerly "Mound Quepos" (Levin et al., 2015) and "Quepos Seep" (Lindgren et al., 2019; McCowin and Rouse, 2018)), and Jaco Scar (Fig. 1, Table 1, Supplementary Table 1). Four *Bathymodiolus thermophilus* specimens were also collected and subsampled for DNA in 2017 and 2019. Three *B. thermophilus* specimens from the East Pacific Rise (collected between 1985 and 2007) were also used for the morphological analyses in this study, and two *"B." manusensis* specimens from the Snowcap dive site in the Manus Basin (collected in 2000) were used in the phylogenetic analyses in this study (Table 1, Supplementary Tables 1 and 3).

For molecular analyses, a portion of the foot was cut and preserved in 95% ethanol (details of individual samples are noted in Material Examined). Specimens were photographed post-preservation with a

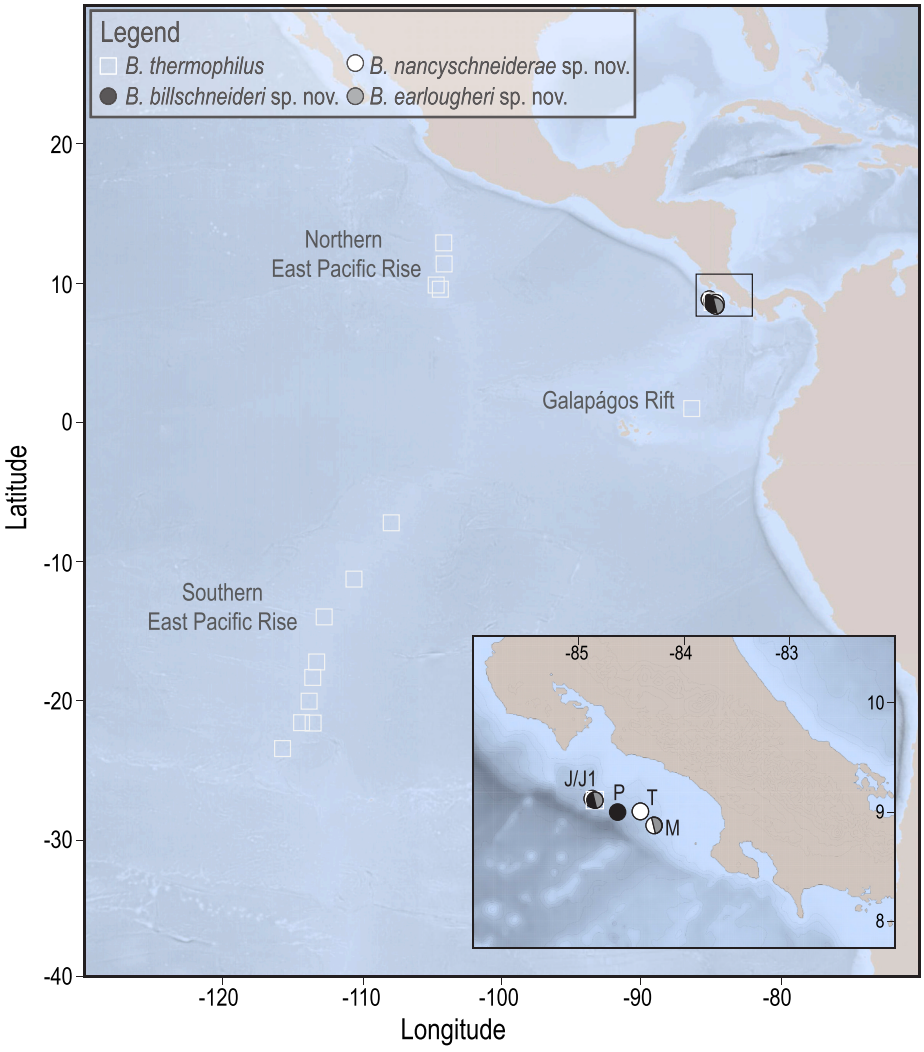

Fig. 1. Distribution of *Bathymodiolus thermophilus* (squares) and three new *Bathymodiolus* species (circles) in the eastern Pacific and along the Costa Rica margin: *Bathymodiolus thermophilus* (white square), *Bathymodiolus billschneideri* n. sp. (black circle), *Bathymodiolus earlougheri* n. sp. (grey circle), *Bathymodiolus nancyschneiderae* n. sp. (white circle). Detailed map of sampling at Costa Rica margin lower right: Jaco Scar (J), Jaco-1000 (J1), Parrita Seep (P), The Thumb (T), Mound 12 (M).

Table 1
Origin of sequenced terminals, vouchers, and GenBank accession numbers used in final concatenated analyses (8 genes). New sequences are set in bold.

Scientific Name	Origin	Habitat	COI	16S	HSP70	ND4	ANT	18S	28S	HH3	Voucher or Reference
"Bathymodiolus "aduloides	Kikajima Island	vent	AB170057	–	–	AB175326	–	–	–	–	Iwasaki et al., 2006
Bathymodiolus antarcticus	EPR	vent	AF456317	–	–	AY649809	–	AY649823	AY781140	–	Won et al., 2003; Jones et al., 2006
Bathymodiolus azoricus	Menez Gwen (Atl.)	vent	AY649795	KF611758	KF720580	–	KF720540	AY649822	AY781148	KF720621	Jones et al., 2006; Thubaut et al., 2013
Bathymodiolus billschneideri n. sp.	**Jaco Scar, CR**	**seep**	**MN986781**	**MN977821**	**-**	**-**	**-**	**MN978735**	**MN978745**	**MN986898**	**SIO-BIC M14535**
Bathymodiolus billschneideri n. sp.	**Jaco Scar, CR**	**seep**	**MN904638**	**MN977822**	**-**	**-**	**-**	**MN978736**	**-**	**-**	**SIO-BIC M12078–04**
Bathymodiolus billschneideri n. sp.	**Jaco Scar, CR**	**seep**	**MN986815**	**MN977823**	**MN986906**	**-**	**MN974019**	**MN978737**	**-**	**-**	**SIO-BIC M16792**
Bathymodiolus boomerang	Barbados Accretionar Prism	seep	FJ890503	KF611759	KF720579	–	KF720541	–	FJ890505	KF720622	Lorion et al., 2010; Thubaut et al., 2013
Bathymodiolus brevior	Mariana Trough	vent	AY649799	–	–	AY649806	–	AY649824	AY781150	–	Jones et al., 2006
Bathymodiolus brooksi	West Florida Escarpment	seep	AY649798	–	–	AY649805	–	AY649825	AY781135	–	Jones et al., 2006
Bathymodiolus earlougheri n. sp.	**Jaco Scar, CR**	**seep**	**MN986856**	**-**	**-**	**-**	**-**	**-**	**-**	**-**	**SIO-BIC M12080**
Bathymodiolus earlougheri n. sp.	**Mound 12, CR**	**seep**	**MN986865**	**MN977824**	**-**	**MN986913**	**-**	**MN978738**	**MN978746**	**MN986899**	**SIO-BIC M14487**
Bathymodiolus earlougheri n. sp.	**Mound 12, CR**	**seep**	**MN986851**	**MN977825**	**MN986907**	**MN986914**	**-**	**MN978739**	**MN978747**	**MN986900**	**SIO-BIC M18326 (M11974–05)**
Bathymodiolus heckerae	West Florida Escarpment	seep	AY649794	–	–	AY130246	–	AF221639	AY781138	–	Jones et al., 2006; Distel et al., 2000
"Bathymodiolus" manusensis	**Manus Basin**	**vent**	**MN986850**	**-**	**-**	**-**	**-**	**MN978740**	**MN978748**	**MN986901**	**SAM D19368.13**
"Bathymodiolus" manusensis	Manus Basin	vent	GU966637	HF545059	KF720556	–	KF720537	KF611718	GU966642	KF720618	Lorion et al., 2010, 2013; Thubaut et al., 2013
Bathymodiolus marisindicus	Edmond, CIR	vent	AY275543	–	–	AY046279	–	AY649818	AY781147	–	Smith et al., 2004; Van Dover et al., 2001; Jones et al., 2006
Bathymodiolus nancyschneiderae n. sp.	**Mound 12, CR**	**seep**	**MN895199**	**-**	**MN986908**	**MN986915**	**-**	**-**	**-**	**-**	**SIO-BIC M18327 (M11979–07)**
Bathymodiolus nancyschneiderae n. sp.	**Mound 12, CR**	**seep**	**MN895191**	**MN977826**	**MN986909**	**MN986916**	**-**	**MN978741**	**MN978749**	**MN986902**	**SIO-BIC M11974–18**
Bathymodiolus nancyschneiderae n. sp.	**Mound 12, CR**	**seep**	**MN895215**	**MN977827**	**MN986910**	**MN986917**	**-**	**MN978742**	**MN978750**	**MN986903**	**SIO-BIC M14471**
Bathymodiolus nancyschneiderae n. sp.	**Jaco-1000, CR**	**seep**	**MN895206**	**MN977828**	**MN986911**	**MN986918**	**MN974020**	**MN978743**	**MN978751**	**MN986904**	**SIO-BIC M12032**
Bathymodiolus puteoserpentis	Snake Pit, MAR	vent/seep	AY649796	–	–	AF128533	–	AF221640	AY781151	–	Maas et al., 1999; Distel et al., 2000; Jones et al., 2006
Bathymodiolus septemdierum	Nankai Trough	seep	AB170052	–	–	AB175298	–	–	–	–	Iwasaki et al., 2006
Bathymodiolus thermophilus	EPR	vent	AF456285	–	–	AY649807	–	AF221638	AY781141	–	Won et al., 2003; Jones et al., 2006; Distel et al., 2000
Bathymodiolus thermophilus	EPR	vent	GU966639	KF611760	–	–	FJ842134	–	GU966640	KF720623	Lorion et al., 2010; Thubaut et al., 2013; Audzijonyte and Vrijenhoek, 2010

(*continued on next page*)

Table 1 (*continued*)

Scientific Name	Origin	Habitat	COI	16S	HSP70	ND4	ANT	18S	28S	HH3	Voucher or Reference
Bathymodiolus thermophilus	**Jaco Scar, CR**	**seep**	**MN986846**	**-**	**MN986912**	**MN986919**	**-**	**MN978744**	**-**	**MN986905**	**SIO-BIC M14568**
Benthomodiolus geikotsucola	Japan	organic substrate	HF545103	HF545049	–	–	–	–	HF545023	HF545149	Lorion et al. (2013)
Benthomodiolus lignocola	New Zealand	organic substrate	AY275545	HF545050	–	AY649817	–	AF221648	AY781131	KF720596	Smith et al., 2004; Lorion et al., 2013; Jones et al., 2006; Distel et al., 2000; Thubaut et al., 2013
Benthomodiolus lignocola	South Atlantic	organic substrate	KF611691	KF611733	KF720560	–	–	KF611703	KF611698	KF720593	Thubaut et al., 2013
Gigantidas childressi	Alaminos Canyon (Atl.)	seep	AY649800	–	–	AY130248	–	AF221641	AY781137	–	Jones et al., 2006; Won et al., 2003; Distel et al., 2000
Gigantidas crypta	Philippines	organic substrate	EU702319	KF611750	KF720563	–	KF720531	KF611714	EU683298	KF720612	Lorion et al., 2009;Thubaut et al., 2013
Gigantidas gladius	Rumble III (WP)	vent	AY649802	–	–	AY649813	–	AY649821	AY781149	–	Jones et al., 2006
Gigantidas hirtus	Kuroshima Knoll	seep	AB170047	–	–	AB175301	–	–	–	–	Iwasaki et al., 2006
Gigantidas japonicus	Mid-Okinawa Trough	seep	AB101422	HF545081	–	AB175281	–	–	HF545039	HF545154	Miyazaki et al., 2004; Lorion et al., 2013; Iwasaki et al., 2006
Gigantidas mauritanicus	West Africa	seep	AY649801	–	–	AY649810	–	AY649828	AY781144	–	Jones et al., 2006
Gigantidas mauritanicus	Barbados Accretionar Prism	seep	FJ890502	KF611747	KF720565	–	KF720528	KF611712	FJ890504	KF720609	Lorion et al., 2010; Thubaut et al., 2013
Gigantidas platifrons	Sagami Bay	vent/seep	AB101420	–	–	AB175286					Miyazaki et al., 2004; Iwasaki et al., 2006
Gigantidas securiformis	Nankai Trough	seep	AB170052	–	–	AB175298	–	–	–	–	Iwasaki et al., 2006
Gigantidas taiwanensis	Okinawa Arc	seep	GU966638	KF611746	KF720566	–	KF720527	KF611711	GU966641	KF720608	Lorion et al., 2010; Thubaut et al., 2013
Gigantidas tangaroa	New Zealand	seep	AY608439	KF611748	KF720572	AY649811	KF720529	AY649820	AY781134	KF720610	Smith et al., 2004; Thubaut et al., 2013; Jones et al., 2006
Idas macdonaldi	Gulf of Mexico	seep	AY649804	–	–	AY649816	–	–	AY781145	–	Jones et al., 2006
Idas washingtonius	Monterey Bay	organic substrate	AY275546	HF545073	–	AY649815	–	AF221645	AY781146	–	Smith et al., 2004; Lorion et al., 2013; Jones et al., 2006; Distel et al., 2000
Tamu fisheri	Garden Banks, GoM	seep	AY649803	–	–	AY649814	–	AF221642	AY781132	–	Jones et al., 2006; Distel et al., 2000
Terua arcuatilis	New Zealand	organic substrate	FJ937033	KF611756	KF720584	–	KF720538	KF611719	GU065879	KF720619	Lorion et al., 2010; Thubaut et al., 2013
Vulcanidas insolatus	Kermadec Ridge, NZ	vent	FJ767936	KF611739	KF720558	–	KF720520	KF611706	FJ767937	KF720601	Lorion et al., 2010; Thubaut et al., 2013
Vulcanidas insolatus (sp. 3)	Kermadec Ridge, NZ	vent	AY608440	–	–	AY649812	–	AY649819	AY781133	–	Smith et al., 2004; Jones et al., 2006

Canon Rebel camera. After subsampling, the holotypes were fixed in 8% formalin. Most of the remaining specimens were cleaned and their shells were dried for preservation. Three paratypes are deposited at the Museo de Zoología, Universidad de Costa Rica, San Jose, Costa Rica (MZUCR), and the holotypes, remaining paratypes, and other collected specimens are deposited in the Scripps Institution of Oceanography Benthic Invertebrate Collection (SIO-BIC), La Jolla, California, USA.

2.2. DNA extraction, amplification, and sequencing

DNA was extracted from 271 *Bathymodiolus* specimens with the Zymo Research DNA-Tissue Miniprep kit, following the protocol supplied by the manufacturer. Approximately 550 bp of the mitochondrial gene cytochrome oxidase subunit I (COI) were amplified for each specimen using the *Bathymodiolus* primers BathCOIF and BathCOIR (Olu-Le Roy et al., 2007), (Supplementary Table 1). For a subset of 12 specimens, up to three additional mitochondrial genes (16S rRNA [16S], NADH dehydrogenase subunit 4 [ND4], and heat shock protein 70 [HSP70]) and up to four nuclear genes (18S rRNA [18S], 28S rRNA [28S], histone H3 [HH3], and adenine nucleotide ADP/ATP translocase [ANT]) were amplified for genetic analysis (Table 1). Amplification details for each gene can be found in Table 2. Fast PCR reactions (COI, 16S, ND4, HSP70, 18S, 28S, HH3) were carried out with the following approximate temperature profiles shown in Table 2, and touchdown PCR was conducted to amplify the ANT gene (same temperature and duration as the Fast PCR for denaturation and extension, but with an annealing temperature that decreased from 55 to 48°/45s; Table 2). All PCR products were purified with the ExoSAP-IT protocol (USB, Affymetrix) and sequencing was performed by Eurofins Genomics (Louisville, KY).

2.3. Molecular analyses

In order to control for doubly uniparental inheritance (DUI), known in some Mytilidae (Breton et al., 2007; Passamonti et al., 2011; Zouros et al., 1994), COI and additional gene sequences for multiple specimens of each species were used in preliminary phylogenetic analyses (Table 1, Supplementary Table 1). We compared sequences from multiple specimens of each species to confirm that there were no "divergent or highly heterogeneous DNA sequences" among the replicates (Fujita et al., 2009; Iwasaki et al., 2006; Kyuno et al., 2009; Miyazaki et al., 2010) that might be indicative of DUI. After this preliminary analysis, a single representative was chosen to represent each species in the final phylogenetic analyses (with a few exceptions where biogeographical relationships were of interest, e.g. *B. thermophilus*). The newly generated sequences plus available sequence data from GenBank for other *Bathymodiolus* species (Table 1) were aligned with MAFFT with default settings (Katoh and Standley, 2013). Poorly-aligned regions of the 16S, 18S, and 28S noncoding genes were removed using Gblocks version 0.91b (Catresana, 2000), with least stringent settings. 93% of sites were retained by Gblocking for 16S, 98% for 18S, and 82% for 28S. This resulted in two alignments for each of these genes, as well as two concatenated alignments, referred to here as complete and Gblocked.

Best-fit models for individual gene alignments (complete and Gblocked, if applicable) were selected using the Akaike information criterion (AIC) in jModelTest 2 (Darriba et al., 2012; Guindon and Gascuel, 2003). All partition models assigned by jModelTest 2 are reported in associated figure legends. Maximum likelihood (ML) analyses were conducted on individual gene alignments (complete and Gblocked, if applicable) separately using the RAxML-HPC2 Workflow on XSEDE v. 8.2.12 in the CIPRES Science Gateway v. 3.3 (Miller et al., 2010; Stamatakis, 2014). A mitochondrial concatenated analysis (COI, 16S, HSP70, ND4; complete and Gblocked) and a nuclear concatenated analysis (18S, 28S, HH3, ANT; complete and Gblocked) were also conducted in RAxML. An ML analysis was conducted for each of the eight-gene concatenated datasets using the same RAxML workflow (and the GTR + G + I model). Node support was assessed via a thorough bootstrapping (1000 replicates) for all ML analyses. Bayesian Inference (BI) analyses were conducted on the complete and Gblocked eight-gene concatenated datasets using MrBayes on XSEDE v. 3.2.x in the CIPRES Science Gateway v. 3.3 (Miller et al., 2010; Ronquist et al., 2012). Each gene partition was assigned the appropriate best-fit model selected by jModelTest 2. Maximum parsimony (MP) analyses were also conducted for the complete and Gblocked eight-gene concatenated datasets using PAUP* v. 4.0a.165 (Swofford, 2002), using heuristic searches with the tree-bisection-reconnection branch-swapping algorithm and 100 random addition replicates. Support values for the MP analyses were determined using 100 bootstrap replicates.

An Approximately Unbiased Test (Shimodaira, 2002) was conducted to test whether one placement of *Bathymodiolus nancyschneiderae* n. sp. in the phylogenetic trees was more likely than the other. A constraint tree placing *B. nancyschneiderae* n. sp. with the clade containing *B. thermophilus*, *B. antarcticus* Johnson and Vrijenhoek, 2013, *B. billschneideri* n. sp., and *B. earlougheri* n. sp. was made using Mesquite v. 3.6 (Maddison and Maddison, 2018) and RAxML v.1.5. Subsequently, IQ-Tree v.1.6.12 (Chernomor et al., 2016) was used to conduct the AU test with 20,000 replicates to generate likelihood scores for the constrained tree and the unconstrained tree (the unconstrained tree from the eight-gene concatenated ML analysis can be seen in Fig. 2). The AU test was also conducted with PAUP* with 10,000 replicates, and the corresponding likelihood scores and p-value were compared with the IQ-Tree results.

Table 2
Amplification details (fragment size, primers and associated references, and amplification programs) for each locus amplified in this study. Touchdown PCR was used to amplify ANT (annealing temperature decreased from 55 to 48 °C over 40 cycles of Denaturation, Annealing Extension. Fast PCR was used to amplify all other loci (30–40 cycles Denaturation, Annealing, Extension). Abbreviations: m - minutes, s - seconds.

Locus	Primers	Approx. Fragment Size (bp)	Initial Denaturation	Denaturation	Annealing	Extension	Final Extension	Reference
COI	BathCOIF, BathCOIR	550	94 °C/4m	94 °C/40s	50 °C/50s	72 °C/1m	72/10m	Olu-Le Roy et al., 2007
16S	Idas16SA, IdasLRJ12864	455	94 °C/4 m	94 °C/40s	55 °C/50s	72 °C/1m	72 °C/10m	Baco-Taylor, 2002; Thubaut et al., 2013
ND4	ND46S, ND47A	490	94 °C/2–4m	94 °C/ 30–40s	52–56.5 °C/ 10–50s	72–74 °C/ 40–60s	72 °C/10m	Kyuno et al., 2009
HSP70	HSP70F, HSP70R	885	94 °C/4m	94 °C/40s	55 °C/50s	72 °C/1m	72 °C/10m	Thubaut et al., 2013
18S	18S1F, 18S5R; 18S9R, 18Sa2.0	1190	94 °C/3m	94 °C/30s	49 °C/30s	72 °C/1m	72 °C/8m	Giribet et al., 1996; Whiting et al., 1997
18S	18S3F, 18Sbi	590	95 °C/3m	95 °C/30s	52 °C/30s	72 °C/90s	72 °C/8m	Giribet et al., 1996; Whiting et al., 1997
28S	28SC1, 28SD2	795	95 °C/3m	95 °C/30s	55 °C/40s	72 °C/75s	72 °C/5m	Jovelin and Justine, 2001
HH3	H3F, H3R	330	95 °C/3m	94 °C/30s	53 °C/45s	72 °C/45s	72 °C/5m	Colgan et al., 1998
ANT	ANTF, ANTR1, ANTR2	500	94 °C/3m	94 °C/30s	55-48 °C/45s	72 °C/1m	72 °C/10m	Audzijonyte and Vrijenhoek, 2010

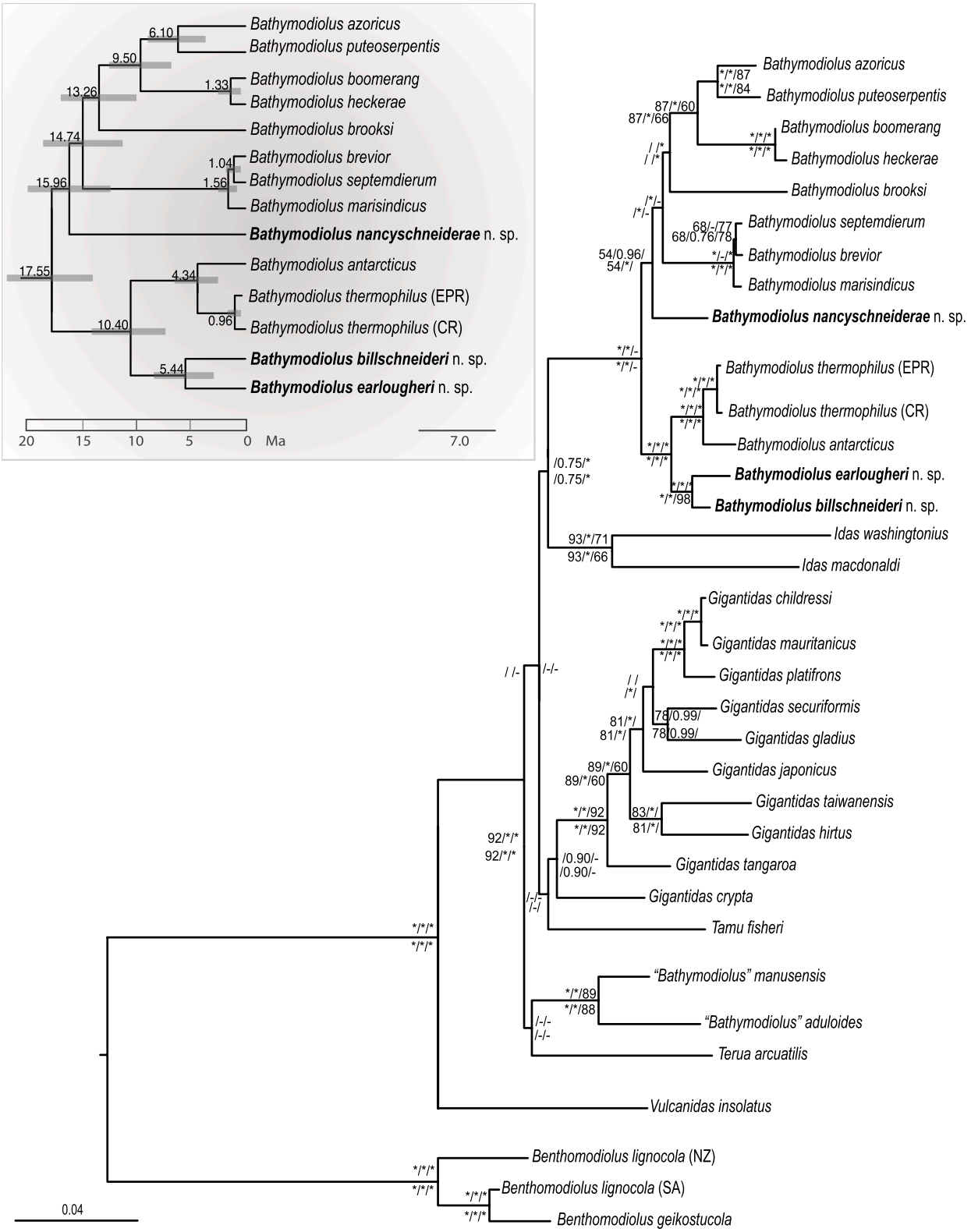

Fig. 2. Maximum likelihood tree of the combined analysis from four mitochondrial (COI, 16S, ND4, HSP70) and four nuclear (18S, 28S, HH3, ANT) genes, conducted in RAxML with best-fit model GTR + G + I. Support values for the complete analysis aligned with MAFFT listed above nodes, support values for the Gblocked analysis listed below nodes. Bootstrap support percentages from Maximum Likelihood analysis, Bayesian posterior probabilities, and bootstrap support percentages from Maximum Parsimony analysis separated by slashes. Support values of 95%/1 or greater for each analysis are indicated by asterisks, support values less than 50%/0.9 are left blank, and nodes not recovered in one of the analyses are indicated by a hyphen. **Inset**. Results of molecular dating analyses (Bayesian inference tree generated with BEAST) for *Bathymodiolus* clade (excluding *"B." aduloides* and *"B." manusensis*), with best-fit models assigned to individual genes (see Supplementary Figs. 2-3 for details). Node ages are indicated above nodes and node bar in light grey indicate 95% HPD).

A subset of the *Bathymodiolus* COI dataset including the new species holotypes and a selection of relevant sequences from GenBank was used to calculate uncorrected and model-corrected (HKY + G) distances and serve as a representative sample (Table 3). Minimum uncorrected pairwise distances were calculated for the entire COI dataset (~400 bp) with PAUP* (Supplementary Table 2). A model-corrected distance analysis for a reduced COI dataset containing the three new *Bathymodiolus* species discussed in this paper and their sister clades (supported by the phylogenetic analyses) was also conducted with the best-fit model, HKY + G (Hasegawa et al., 1985), which was selected via AIC in jModelTest 2 (minimum corrected distances represented by bold values in Supplementary Table 2).

Haplotype networks were created using the COI dataset (terminals listed in Supplementary Table 1) for each of the three new *Bathymodiolus* species and *Bathymodiolus thermophilus* with PopART v.1.7 (Bandelt et al., 1999; Leigh and Bryant, 2015) using the median-joining option with epsilon set at 0 for each analysis.

The complete eight-gene concatenated ML phylogeny was also used in an ancestral state reconstruction of habitat. A habitat character with three states, vent, seep, and organic fall, was mapped onto the ML phylogeny using the Mk-1 likelihood model in Mesquite. Where individual taxa had been reported at multiple habitats, multiple states were coded (e.g., vent/seep for a single taxon reported from both habitats).

The complete eight-gene concatenated alignment was used for molecular dating with BEAST2 (v.2.4.8) (Bouckaert et al., 2019) with the same parameter settings as the most recent molecular dating analysis of Bathymodiolinae by Lorion et al. (2013). The tree was minimally constrained to match the complete concatenated ML tree at nodes of interest for molecular dating. A Yule speciation model was used as a tree prior, with rate variation modelled among lineages by an uncorrelated lognormal relaxed clock, with the mean substitution rate fixed to 1. Three fossils were used as calibrations per Lorion et al. (2013) and implemented as prior distributions for node ages in the tree. These fossils include *Vulcanidas goederti* (Kiel and Little, 2006; Lorion et al., 2013), which was dated to the Middle Eocene, 45 Myr (Kiel and Little, 2006); *Gigantidas coseli* (Lorion et al., 2013; Saether et al., 2010), which was dated to the Middle Miocene, 12.7–15.1 Myr (Saether et al., 2010); and *Bathymodiolus heretaunga* (Lorion et al., 2013; Saether et al., 2010), which was dated to the Early Miocene, 21.7–25.2 Myr (Saether et al., 2010). As in Lorion et al. (2013), we modelled the divergence time of the most inclusive clade containing *Vulcanidas insolatus* Cosel and Marshall (2010) using an exponential prior with a hard minimum bound of 45 Myr and a mean of 1.2 Myr, we modelled the divergence time of the most inclusive clade containing *Gigantidas crypta* (Dall et al., 1938) using an exponential prior with a minimum bound of 15.1 Myr and a mean of 1.3 Myr, and we modelled the divergence time of the most inclusive clade containing *Gigantidas childressi* Gustafson et al. (1998) using an exponential prior with a minimum bound of 25.2 Myr and a mean of 0.7 Myr (Lorion et al., 2013). A minimum of four runs of 20 million Markov chain Monte Carlo (MCMC) steps and a 4000-step subsampling of individual runs was used for the analysis. Each of the fossil calibrations was used in a separate analysis to check whether specific fossils had significant influences on the resulting dates (four to eight runs per fossil until a minimum of four runs converged), then a combined analysis with all three calibrations at once was conducted with a total of seven runs: four of these runs converged and were used (3 reached stationarity at a poorer likelihood plateau and were not used). Burn-in was determined to be 15% using Tracer v.1.7 (Rambaut et al., 2018). Runs were combined in LogCombiner and trees were annotated in TreeAnnotator (BEAST v.2.4.8). The combined individual runs and the single combined run yielded nearly identical results. The divergence times of clades of interest were compared with those found in the Lorion et al. (2013) and Johnson et al. (2013) analyses.

Table 3
Uncorrected and corrected distances for a subset of the COI data (new *Bathymodiolus* species holotypes and other relevant *Bathymodiolus* species). Corrected distances (HKY + G) for are set in bold.

	B. billschneideri n. sp.	*B. earlougheri* n. sp.	*B. nancyschneiderae* n. sp.	*B. thermophilus* (EPR)	*B. thermophilus* (CR)	*B. antarcticus*	*B. azoricus*	*B. boomerang*	*B. heckerae*	*B. marisindicus*
B. billschneideri n. sp.	–	**0.0959**	**0.1393**	**0.1022**	**0.1264**	**0.1334**	**0.2191**	**0.2137**	**0.2476**	**0.1797**
B. earlougheri n. sp.	0.0624	–	**0.1672**	**0.1519**	**0.1658**	**0.1737**	**0.2035**	**0.2451**	**0.2561**	**0.1798**
B. nancyschneiderae n. sp.	0.0812	0.0904	–	**0.1805**	**0.1734**	**0.2125**	**0.1846**	**0.1499**	**0.1703**	**0.1583**
B. thermophilus (EPR)	0.0674	0.0851	0.0952	–	**0.0137**	**0.0550**	**0.2723**	**0.2792**	**0.3299**	**0.2139**
B. thermophilus (CR)	0.0763	0.0895	0.0933	0.0127	–	**0.0601**	**0.2448**	**0.2926**	**0.3379**	**0.2172**
B. antarcticus	0.0795	0.0918	0.1037	0.0421	0.0450	–	**0.3022**	**0.2780**	**0.2970**	**0.2158**
B. azoricus	0.1131	0.1069	0.1019	0.1264	0.1194	0.1325	–	**0.1242**	**0.1548**	**0.2614**
B. boomerang	0.1071	0.1152	0.0887	0.1241	0.1261	0.1242	0.0772	–	**0.0131**	**0.2447**
B. heckerae	0.1165	0.1191	0.0963	0.1341	0.1358	0.1280	0.0914	0.0123	–	**0.2296**
B. marisindicus	0.0997	0.1003	0.0902	0.1084	0.1101	0.1098	0.1213	0.1140	0.1119	–
B. septemdierum	0.1133	0.1047	0.0929	0.1128	0.1060	0.1061	0.1187	0.1115	0.1146	0.0220

2.4. Morphological analyses

Identification of the *Bathymodiolus* mussels from Costa Rica seeps by morphology alone was difficult, so morphological identifications were confirmed with DNA sequencing (minimally COI). Of the DNA-confirmed specimens, a subset of the largest shells for each species were used for morphological analyses. Electric calipers (Mitutoyo) accurate to 0.01 mm were used to measure 23 shells of *B. billschneideri* n. sp., 22 shells of *B. nancyschneiderae* n. sp., 13 shells of *B. earlougheri* n. sp., and 7 shells of *B. thermophilus* (including the three specimens from the East Pacific Rise that had been previously identified without DNA evidence). Shell length, shell width, and shell height were measured according to Kenk and Wilson (1985) (Supplementary Table 3) for each specimen. When possible, both valves were measured separately and averaged for each specimen, but for specimens with only a single valve preserved, that valve only was measured (since the taxa measured in this study are equivalve). Prior to any analysis, all data was standardized and zero-centered (z-scores) in RStudio v.1.2.1335 to remove size-related variation in shell shape. Following standardization, a principle component analysis (PCA) was conducted in RStudio using ggplot2 (Wickham, 2016), ggfortify (Tang et al., 2016), factoextra (Kassambara and Mundt, 2019), and FactoMineR (Le et al., 2008) to explore the morphometric data by comparing the three shell morphological measurements.

3. Results

3.1. Molecular analyses

The ML and BI analyses for the complete and Gblocked eight-gene concatenated datasets (Fig. 2) were nearly identical, with some variation at poorly supported nodes. The complete and Gblocked MP analyses yielded similar results to the ML and BI analyses but differed from them at poorly supported nodes. All analyses recovered a *Gigantidas* clade and a *Bathymodiolus* clade (excluding *"B." manusensis* and *"B." aduloides*). The concatenated mitochondrial phylogeny differed noticeably (Supplementary Fig. 1); however, there was also conflict between individual gene trees: not all mitochondrial gene trees agreed with one another or the concatenated mitochondrial tree, and not all nuclear gene trees agreed with one another or the concatenated nuclear tree (Supplementary Figs. 1-3). Interspecific uncorrected pairwise distances among *Bathymodiolus* species (excluding *"B." manusensis* and *"B." aduloides*) ranged from 2.09 to 18.37% and the corrected pairwise distances ranged from 2.35 to 35.98% (Supplementary Table 2).

All concatenated analyses (ML, BI, MP) consistently placed *Bathymodiolus billschneideri* n. sp. sister to *B. earlougheri* n. sp. with high support (Fig. 2). This clade was recovered as sister to the clade containing *B. thermophilus* and *B. antarcticus* with maximal support in all concatenated analyses. The concatenated mitochondrial, concatenated nuclear, and individual gene trees also consistently recovered the close sister relationship between *B. billschneideri* n. sp. and *B. earlougheri* n. sp. (Supplementary Figs. 1-3). Most gene trees also recovered the close relationship between *B. thermophilus* and either/both *B. billschneideri* n. sp. and *B. earlougheri* n. sp. (COI, 16S, ND4, HSP70, 18S, 28S, HH3; Supplementary Figs. 2-3). Uncorrected pairwise distances for the COI dataset showed that *B. billschneideri* n. sp. and *B. earlougheri* n. sp. had a minimum divergence of 5.65% from one another (Supplementary Table 2) and the holotypes were 6.24% divergent from one another (Table 3). Both *B. billschneideri* n. sp. and *B. earlougheri* n. sp. also exhibited small uncorrected distances from *B. thermophilus* (9°N haplotype): minimally 6.85% and 8.08% respectively (Table 3, Supplementary Table 2). Model-corrected pairwise distances for a subset of the COI data (*Bathymodiolus* clade only) revealed similar, though larger, relative distances (Table 3, Supplementary Table 2). *Bathymodiolus billschneideri* n. sp. and *B. earlougheri* exhibited a next-closest relationship to *B. thermophilus* (Table 3, Supplementary Table 2). *Bathymodiolus antarcticus*, the sister taxon to *B. thermophilus,* was also closely related to *B. billschneideri* n. sp. and *B. earlougheri* n. sp. (Table 3, Supplementary Table 2).

The ML and BI (concatenated) analyses recovered *Bathymodiolus nancyschneiderae* n. sp. as sister, with low support, to a clade of mixed Pacific, Atlantic, and Indian Ocean taxa that was distinctly separate from the East Pacific taxa, (Fig. 2). The placement of *B. nancyschneiderae* n. sp. was variable across the gene trees (Supplementary Figs. 1-3). The concatenated mitochondrial tree (Supplementary Fig. 1A) recovered *B. nancyschneiderae* as sister to the clade containing the East Pacific taxa *B. thermophilus*, *B. antarcticus*, *B. billschneideri* n. sp., and *B. earlougheri* n. sp. In contrast, the concatenated nuclear tree (Supplementary Fig. 1B) recovered the same placement of *B. nancyschneiderae* n. sp. as the ML and BI analyses. There was not a consistent topology trend associated with mitochondrial or nuclear loci and disagreements between loci were at nodes with poor support. However, most gene trees showed a close relationship between *B. billschneideri* n. sp. and *B. earlougheri* n. sp. that was distinctly separate from *B. nancyschneiderae* n. sp. (Supplementary Figs. 1-3). Since the placement of *B. nancyschneiderae* n. sp. in the eight-gene concatenated ML tree (with the non-East-Pacific taxa) differed from its placement in the concatenated mitochondrial analysis and some of the gene trees, an Approximately Unbiased Test (AU Test), was conducted to compare the original ML tree (seen in Fig. 2) with a constrained ML tree that placed *B. nancyschneiderae* n. sp. with the East Pacific clade. Two AU tests, conducted independently in IQ-Tree and PAUP*, recovered no significant difference between the trees, with p-values of 0.201 and 0.223, respectively. Uncorrected pairwise distances for the COI dataset revealed that *B. nancyschneiderae* n. sp. was minimally 7.52% and 8.08% divergent from *B. billschneideri* n. sp. and *B. earlougheri* n. sp. respectively (Supplementary Table 2). The *B. nancyschneiderae* n. sp. holotype was 8.12% and 9.04% divergent from the *B. billschneideri* n. sp. and *B. earlougheri* n. sp. holotypes respectively (Table 3). *Bathymodiolus nancyschneiderae* n. sp. also exhibited a small uncorrected distance from *B. boomerang* (Table 3, Supplementary Table 2). Model-corrected pairwise distances for the COI data subset revealed similar relationships to the uncorrected dataset for *B. nancyschneiderae* n. sp. (Table 3, Supplementary Table 2): *B. nancyschneiderae* n. sp. was minimally 11.39% and 12.84% divergent from *B. billschneideri* n. sp. and *B. earlougheri* n. sp. respectively (holotypes 13.93% and 16.72% divergent respectively) (Table 3, Supplementary Table 2). Though *B. billschneideri* n. sp. exhibited a smallest minimum corrected distance from *B. nancyschneiderae* n. sp. (above), *B. marisindicus* was also very close to *B. nancyschneiderae* n. sp. (minimum corrected distance of 13.37%) (Supplementary Table 2).

Bathymodiolus thermophilus was recovered as sister to *B. antarcticus* with maximal support in all concatenated analyses (Fig. 2). This clade was recovered as sister to *B. billschneideri* n. sp. and *B. earlougheri* n. sp. also with high support in all concatenated analyses (Fig. 2). *Bathymodiolus thermophilus* samples from Costa Rica were recovered as sister to a confirmed *B. thermophilus* specimen from the East Pacific Rise with a very short branch length and maximal support from all concatenated analyses (Fig. 2) and in all gene trees for which there was sequence data available for both terminals (Supplementary Figs. 2-3). The uncorrected distance analysis (based on the COI dataset) revealed that the *B. thermophilus* specimens sampled from Costa Rica were 0–2.11% divergent from the other *B. thermophilus* sequences (from the East Pacific Rise and the Galápagos Rift) (Table 3, Supplementary Table 2). The corrected distance analysis (based on a subset of the COI data) revealed similar distances (Table 3, Supplementary Table 2). Measurements of the shells of *B. thermophilus* specimens from Costa Rica and the East Pacific Rise resulted in a slight extension of the previously recorded shell measurements for this species. The mean ratio of height to length in specimens from Costa Rica was 0.416; range 0.391–0.430 (previously 0.475, range 0.428–0.513). The mean ratio of width to length in specimens from Costa Rica was 0.137; range 0.124–0.147 (previously 0.208; range of 0.185–0.230).

Haplotype networks generated from the COI data (sequences 450–520 bp in length) for each new species revealed similar network

shapes: within each species there was a single dominant haplotype, with other haplotypes varying by just a few base pairs (Fig. 3). In total, there were 66 *B. billschneideri* n. sp. sequences, 150 *B. nancyschneiderae* n. sp. sequences, 45 *B. earlougheri* n. sp. sequences, and 41 *B. thermophilus* sequences. The COI haplotype network for *B. billschneideri* n. sp. showed that the majority of specimens shared a single haplotype regardless of locality/depth, with a few specimens differing by at most a few base pairs (Fig. 3). However, *B. billschneideri* n. sp. appeared to be restricted to two localities/depths: Jaco Scar (1800 m) and Parrita Seep (1400 m). The *B. earlougheri* n. sp. haplotype network exhibited a similar structure with a single haplotype shared by the majority of specimens regardless of locality (Fig. 3). *Bathymodiolus earlougheri* n. sp. was present at the shallower sampling sites Mound 12 (1000 m) and The Thumb (1060 m), as well as the deepest sampling site, Jaco Scar (1800 m), but not at Parrita Seep (1400 m) (Fig. 3). *Bathymodiolus nancyschneiderae* n. sp. shared the same network shape but was not sampled below 1100 m; it was only present at the three shallowest sampling sites: Mound 12 (1000 m), The Thumb (1070 m) and Jaco-1000 (1060 m) (Fig. 3). The haplotype network generated from the COI data for *B. thermophilus* (Fig. 4, ~400 bp), which included a subset of sequences from East Pacific Rise and Galápagos Rift (Johnson et al., 2013) revealed that the five Costa Rican seep *B. thermophilus* sequences were either of two previously established dominant haplotypes from Johnson et al. (2013). One of the haplotypes (including four Costa Rica specimens) was shared with *B. thermophilus* sequences from vents at the northern East Pacific Rise and southern East Pacific Rise, while the other dominant haplotype (including one Costa Rica specimen) was shared with *B. thermophilus* sequences from vents at the Galápagos Rift, northern East Pacific Rise, and southern East Pacific Rise. These two haplotypes diverged by approximately six base pairs from one another (Fig. 4).

The maximum clade credibility tree created with the Bayesian relaxed-clock analysis (calibrated using fossils at three nodes; converged runs that were conducted with individual fossils did not vary significantly from the combined runs) resulted in an estimated mean age for the most recent common ancestor for *Bathymodiolus* (excluding *"B." manusensis* and *"B." aduloides*) of 17.5 Myr (95% HPD interval: 13.67–21.47) (Fig. 2 inset; see Supplementary Fig. 4 for full time tree). Our analysis calculated an estimated mean age of 4.34 Myr (95% HPD interval: 2.47–6.44 Myr) for the divergence of *B. thermophilus* and *B. antarcticus*, which was previously calculated by Lorion et al. (2013) and Johnson et al. (2013) to be approximately 5 Myr and 2.1–4.3 Myr,

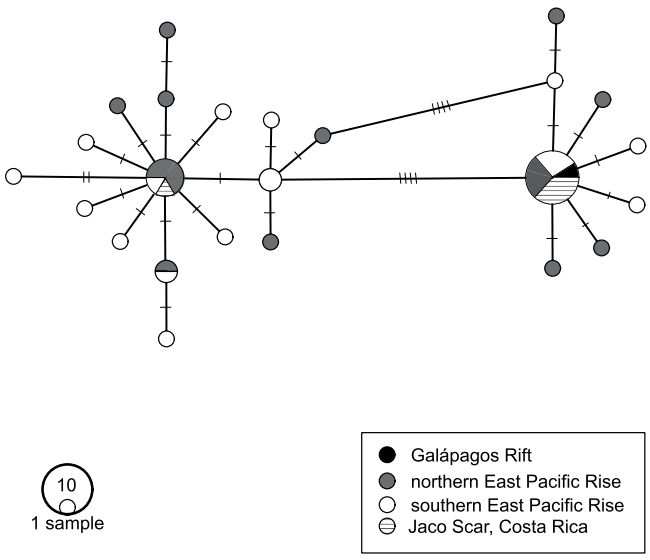

Fig. 4. Haplotype network from COI data for *Bathymodiolus thermophilus*. Color-coded according to locality.

respectively. The estimated mean age for the divergence of *B. billschneideri* n. sp. and *B. earlougheri* n. sp. from the *B. thermophilus/antarcticus* clade was 10.4 Myr (95% HPD interval: 7.23–13.94). The estimated mean age for the divergence of *B. billschneideri* n. sp. from *B. earlougheri* n. sp. was 5.44 Myr (95% HPD interval: 2.85–8.30), and the estimated mean age for the divergence of *B. nancyschneiderae* n. sp. from the other *Bathymodiolus* clade (including *B. marisindicus* and *B. azoricus* Cosel and Comtet, 1999) was 15.95 Myr (95% HPD interval: 12.22–19.74) (Supplementary Fig. 4).

The likelihood ancestral state reconstruction revealed that a seep origin was most likely for the most recent common ancestor of the *Bathymodiolus* clade, excluding *"B." manusensis* and *"B."aduloides* (Fig. 5). Within *Bathymodiolus*, the East Pacific Rise clade containing *B. thermophilus*, *B. antarcticus*, *B. billschneideri* n. sp., and *B. earlougheri* n. sp. was also most likely to have had an ancestor with a seep origin, similarly to its sister clade containing various *Bathymodiolus* species from the Atlantic, West Pacific, Indian Ocean, Caribbean, Gulf of Mexico, and *B. nancyschneiderae* n. sp. from the East Pacific. The habitat

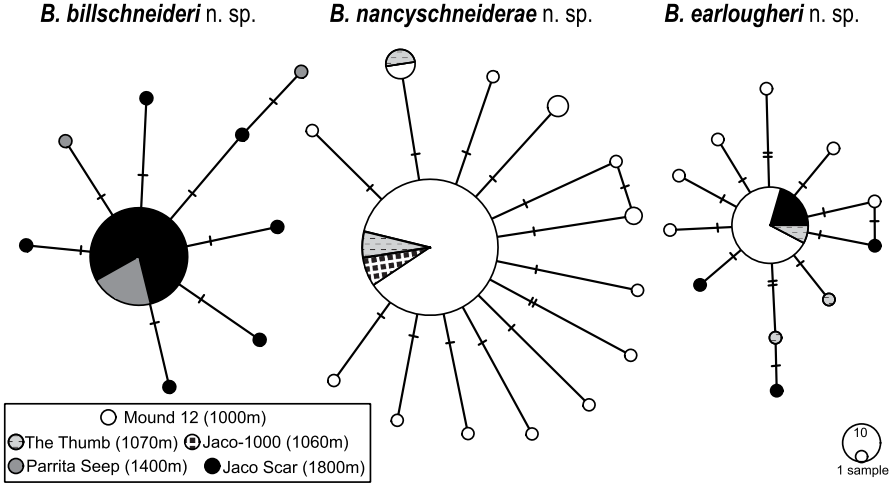

Fig. 3. Haplotype networks from COI data for *Bathymodiolus billschneideri* n. sp., *B. nancyschneiderae* n. sp., and *B. earlougheri* n. sp. Color-coded according to locality/depth of sampling.

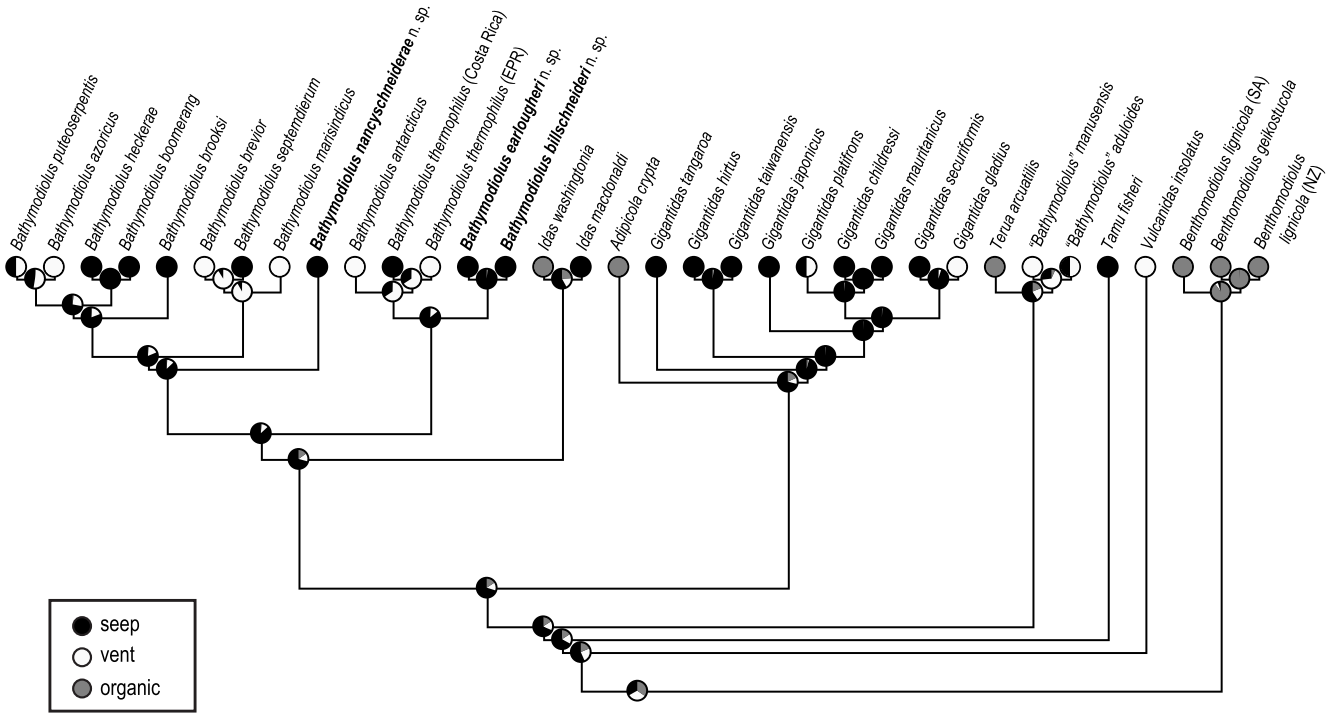

Fig. 5. Likelihood ancestral state reconstruction of habitat (vent, seep, organic fall) mapped onto the complete concatenated ML phylogeny.

of the most recent common ancestor of Bathymodiolinae was ambiguous (Fig. 5).

3.2. Morphological analyses

A morphological examination of the shells of the three new species revealed that *B. earlougheri* n. sp. had a distinguishable shape and color from the other *Bathymodiolus* species sampled from the seeps along the Costa Rica margin. *Bathymodiolus earlougheri* n. sp. shells had a distinct golden-yellow color in all specimens, with a noticeably shorter shell length (relative to shell height and width) and more compact shape than *B. billschneideri* n. sp., *B. nancyschneiderae* n. sp, and *B. thermophilus* (Figs. 6–9). *Bathymodiolus billschneideri* n. sp., *B. nancyschneiderae* n. sp., and *B. thermophilus* could not be reliably differentiated morphologically

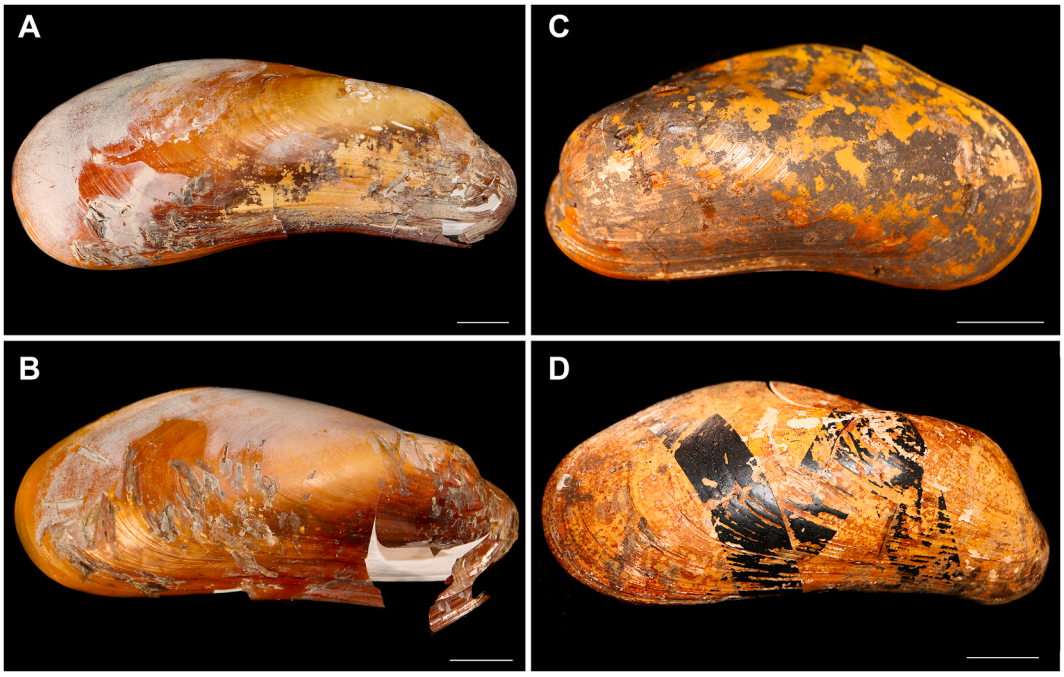

Fig. 6. Photographs of shells of *Bathymodiolus thermophilus*. **A.** SIO-BIC M14586, right valve exterior, sampled from Costa Rica (Jaco Scar). **B.** SIO-BIC M14568, right valve exterior, sampled from Costa Rica (Jaco Scar). **C.** SIO-BIC M16462, left valve exterior, sampled from East Pacific Rise. **D.** SIO-BIC M8223, right valve exterior, sampled from Galápagos Rise. Scale bars indicate 20 mm.

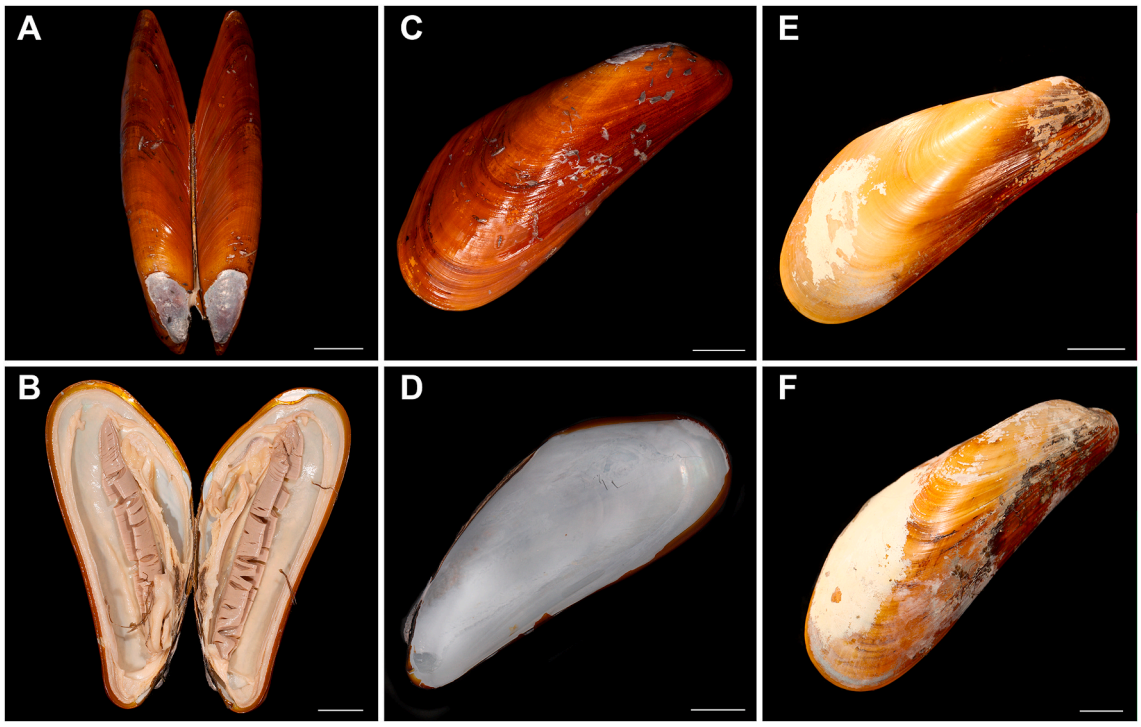

Fig. 7. Photographs of shells and internal anatomy of Bathymodiolus billschneideri n. sp. A. Holotype (SIO-BIC M12074), dorsal exterior. B. Holotype, internal anatomy, ventral view. **C.** Holotype, right valve exterior. **D.** Holotype, right valve interior. **E.** Paratype (SIO-BIC M16763), right valve exterior. **F.** Paratype (SIO-BIC M16793) right valve exterior. Scale bars indicate 20 mm.

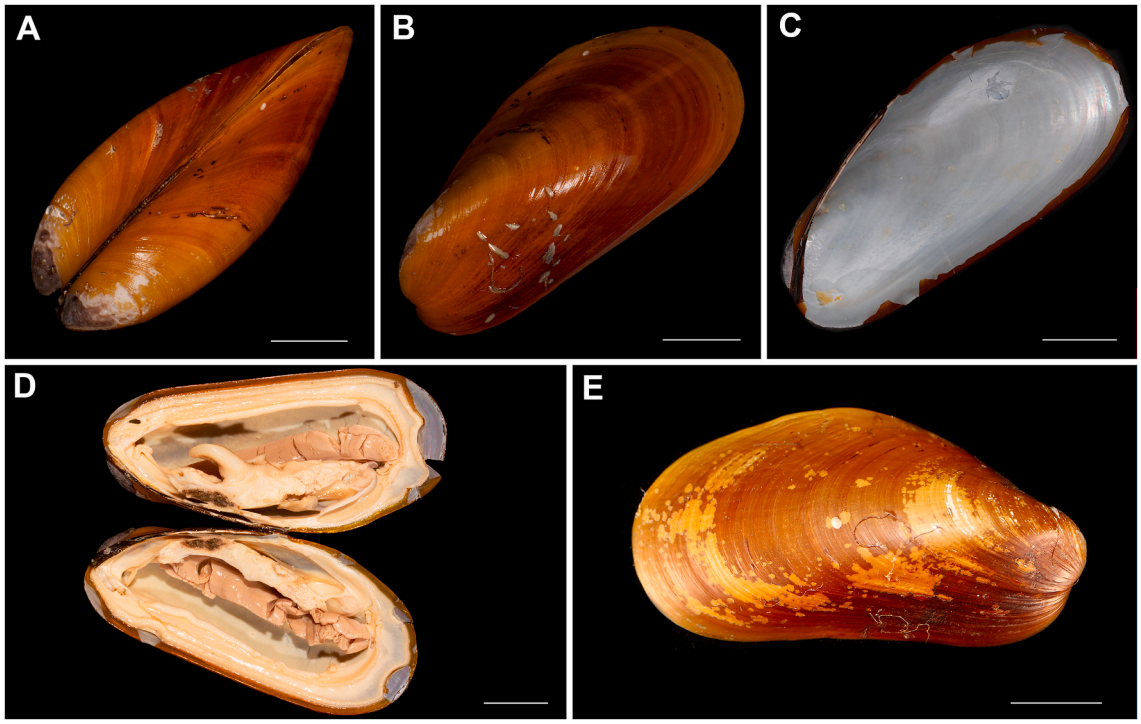

Fig. 8. Photographs of shells and internal anatomy of *Bathymodiolus earlougheri* n. sp. **A.** Holotype (SIO-BIC M12076), dorsal exterior. **B.** Holotype, left valve exterior. **C.** Holotype, right valve interior. **D.** Holotype, internal anatomy, ventral view. **E.** Paratype (SIO-BIC M14479), right valve exterior. Scale bars indicate 20 mm.

and molecular data was required for identification. A Principal Component Analysis (PCA) confirmed the results of the morphological examination, showing that *B. earlougheri* n. sp. could be differentiated reliably from the other two new *Bathymodiolus* species by its more compact shape and golden-yellow color, but that *B. billschneideri* n. sp., *B. nancyschneiderae* n. sp., and *B. thermophilus* could not be differentiated from one another based on shell length, width, or height (Fig. 10). The PCA explained nearly all of the variation (approximately 96%) in the morphological measurements for the shells (shell length, height, and width) of *Bathymodiolus billschneideri* n. sp., *B. earlougheri* n. sp.,

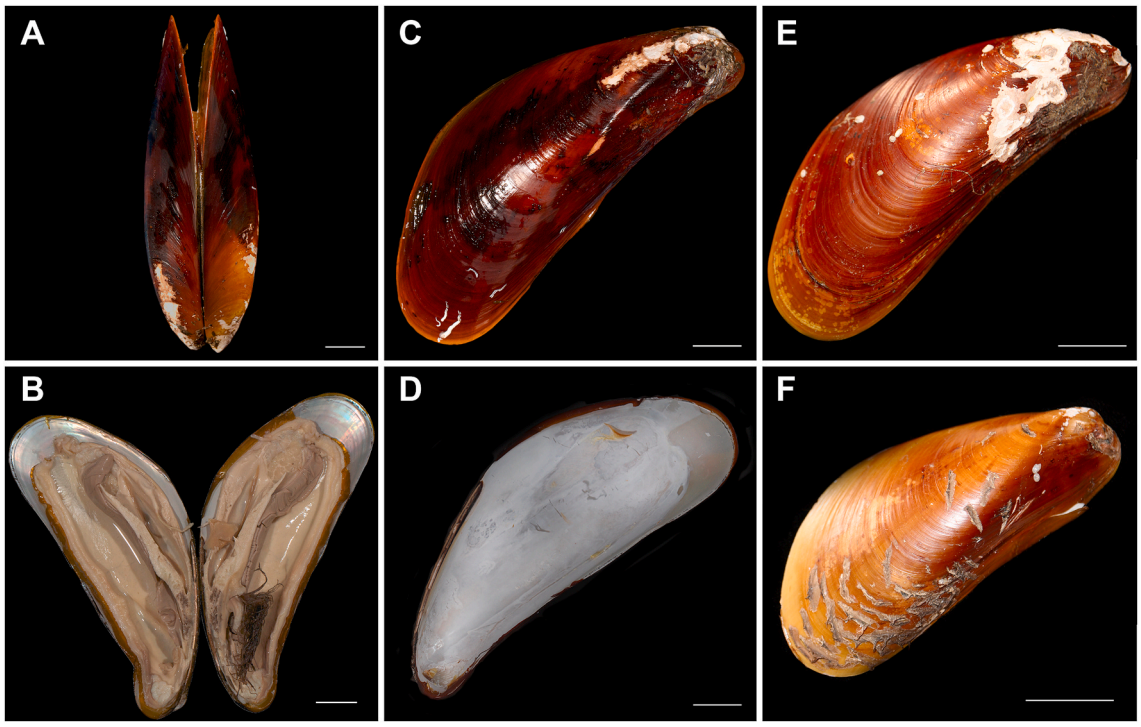

Fig. 9. Photographs of shells and internal anatomy of *Bathymodiolus nancyschneiderae* n. sp. A. Holotype (SIO-BIC M12032), dorsal exterior. B. Holotype, internal anatomy, ventral view. **C.** Holotype, right valve exterior. **D.** Holotype, right valve exterior. **E.** Paratype (SIO-BIC M14531), right valve exterior. **F.** Paratype (SIO-BIC M14530), right valve exterior. Scale bars indicate 20 mm.

B. nancyschneiderae n. sp., and *B. thermophilus* (Fig. 10). PC1 explained approximately 80.1% of the data, and PC2 explained approximately 16.4% of the data (Fig. 10). The relative contributions of shell length, height, and width were 33.3%, 27.1%, and 39.6% (respectively) to PC1, and 33.3%, 1.9%, and 64.8% (respectively) to PC2. *Bathymodiolus thermophilus* (Fig. 6) formed two clusters in the PCA: one that was closer to *B. earlougheri* n. sp. (composed of specimens from the East Pacific Rise) and one that was mixed with *B. billschneideri* n. sp. and *B. nancyschneiderae* n. sp. (specimens from Costa Rica).

4. Discussion

4.1. Molecular analyses

The phylogenetic and distance analyses supported the recognition of three new *Bathymodiolus* species: *B. billschneideri* n. sp., *B. earlougheri* n. sp., and *B. nancyschneiderae* n. sp. (formally described in Taxonomy section) and confirmed the presence of *B. thermophilus* at the Costa Rica seeps. The eight-gene concatenated analyses (ML, BI, MP; complete and Gblocked; Fig. 2) from this study were largely consistent with previous concatenated analyses where nodes were well-supported (Lorion et al., 2013; Thubaut et al., 2013; Xu et al., 2019). The respective monophyly of *Gigantidas* (established by Samadi et al., 2015; Thubaut et al., 2013; Xu et al., 2019) and *Bathymodiolus* (Xu et al., 2019), excluding *"B." manusensis* and *"B." aduloides*, were recovered in all concatenated analyses (Fig. 2). However, our analyses showed some deviation from previous ones at poorly supported nodes. *Bathymodiolus brooksi* Gustafson et al. (1998), *B. brevior*, and *B. azoricus* were always recovered in *Bathymodiolus* and were consistent with Lorion et al. (2013), but their placement within *Bathymodiolus* received low support, varied between analyses, and deviated from Thubaut et al. (2013) and Xu et al. (2019). The placement of *B. nancyschneiderae* n. sp. sister to the non-East-Pacific *Bathymodiolus* species (including *B. azoricus* and *B. septemdierum*) was not well-supported in the ML or MP analyses but was well-supported by the BI analyses (complete and Gblocked). The results of the AU test also showed that the placement of *B. nancyschneiderae* n. sp. sister to the non-East-Pacific *Bathymodiolus* species was not significantly more likely than its placement sister to the East Pacific *Bathymodiolus* species (recovered in the concatenated mitochondrial tree, Supplementary Fig. 1A). This lack of phylogenetic support makes it difficult to ascertain the exact placement of *B. nancyschneiderae* n. sp. in the phylogeny of Bathymodiolinae. However, the phylogeny and minimum distances between *B. nancyschneiderae* n. sp. and its close relatives support its recognition as a new species.

The inclusion of the *Bathymodiolus thermophilus* sample from Costa Rica within *B. thermophilus* was supported by all phylogenetic analyses, distance analyses, and haplotype networks. The samples from Costa Rica exhibited small uncorrected and corrected distances from other available *B. thermophilus* sequences (East Pacific Rise and Galápagos Rift) that were within the expected range for the intraspecific variation of *B. thermophilus*. The COI haplotype network (Fig. 4) of *B. thermophilus* revealed that the Jaco Scar specimens shared two haplotypes with previously sampled specimens from the Galápagos Rift and the East Pacific Rise (940–2300 km away, respectively). This is unsurprising given that *B. thermophilus* specimens from a variety of locations (spanning ~4000 km) along the East Pacific Rise and Galápagos Rift have been shown to share single haplotypes (Johnson et al., 2013), and that *Bathymodiolus* have the capacity for long-distance distance dispersal (Arellano and Young, 2009; Kyuno et al., 2009; Johnson et al., 2013; Arellano et al., 2014). We now confirm records of *B. thermophilus* from the Jaco Scar seep (9.1175°N, 84.8395°W), at depths of 1794–1817 m (Levin et al., 2012).

4.2. Habitat, biogeography, and evolutionary origins of Costa Rica *Bathymodiolus*

The haplotype networks for each of the new species revealed some separation of species by depth along the Costa Rica margin. *Bathymodiolus nancyschneiderae* n. sp. was present only at the shallower dive sites around 1000 m, despite its geographic proximity (less than 1 km) to

deeper sites like Jaco Scar. *Bathymodiolus billschneideri* n. sp. was present at both intermediate sites (Parrita Seep ~1400 m) and deep sites, (Jaco Scar ~1800 m), but was never found at any of the shallower dive sites (Mound 12, The Thumb, Jaco-1000), despite their geographic proximity. *Bathymodiolus earlougheri* n. sp. was present at some of the shallowest sites (1000–1070 m) and deepest sites (1800 m) (Fig. 3) but was not found at any intermediate depths. Each of the haplotype networks for the new *Bathymodiolus* species exhibited a star-shape in which a single haplotype was much more frequent than the others, which is suggestive of a past evolutionary bottleneck (Bazin et al., 2006; Plouviez et al., 2009). In contrast, the reduced-representation haplotype network of *B. thermophilus* (Fig. 4) showed two closely related haplotypes that were more frequent than the others. This finding is consistent with the COI haplotype networks for *B. thermophilus* by Johnson et al. (2013).

The separation of *B. nancyschneiderae* n. sp. from *B. billschneideri* n. sp./*B. earlougheri* n. sp. indicated by some of the molecular analyses suggests it may have a different biogeographic origin from the other *Bathymodiolus* species at the Costa Rica margin. *Bathymodiolus billschneideri* n. sp. and *B. earlougheri* n. sp. were grouped with high support into a clade with *B. thermophilus* and *B. antarcticus* that is sister to the other *Bathymodiolus* species, (Fig. 2). This clearly suggests a Pacific origin for *B. billschneideri* n. sp. and *B. earlougheri* n. sp. However, *B. nancyschneiderae* appeared in the ML and BI analyses to be more closely related to taxa from a variety of other places, including the Atlantic, Indian, and West Pacific oceans. The stratification by depth of *B. nancyschneiderae* n. sp. (only found at ~1000 m) versus *B. billschneideri* n. sp. (only found at 1400–1900 m) may also represent evidence of a different origin. Some of the taxa that *B. nancyschneiderae* n. sp. is closely related to are prevalent in the Gulf of Mexico (*B. brooksi*, *B. heckerae* Gustafson et al., 1998), Caribbean (*B. boomerang*), and Mid-Atlantic Ridge (*B. puteoserpentis* Cosel, Métivier & Hashioto, 1994; *B. azoricus*). Other taxa that exhibit this phylogenetic pattern, such as the vesicomyid *Abyssogena* Krylova, Sahling & Janssen, 2010, the ampharetid *Amphisamytha fauchaldi* Solis-Weiss and Hernandez-Alcantara, 1994, and the annelid *Lamellibrachia donwalshi* McCowin and Rouse, 2018, are hypothesized to have had ancestors that spanned the open seaway between the Pacific and Atlantic and speciated during the shoaling up of deep water that occurred as the Panama Isthmus began to form (Stiller et al., 2013; O'Dea et al., 2016; LaBella et al., 2017). *Amphisamytha fauchaldi*, which was sampled from seeps along the East Pacific margin including Costa Rica, was shown to have a sister taxon from as far as the Mid-Atlantic Ridge (Stiller et al., 2013). Four species of polynoid scaleworms belonging to *Branchipolynoe* Pettibone, 1984 were recently described, and are all symbionts of the *Bathymodiolus* mussels described here (Lindgren et al., 2019). There was no distinct correlation between the divergence patterns of the scaleworms and their mussel hosts. Two of these scaleworms were shown to be most closely related to another species of *Branchipolynoe* from the Gulf of Mexico, rather than to Pacific *Branchipolynoe,* but they are not specific to *B. nancyschneiderae* n. sp. However, the *Bathymodiolus* clade that *B. nancyschneiderae* n. sp. was recovered as sister to also contains taxa sampled from the Central Indian Ridge (*B. marisindicus*) and the Northwest Pacific (*B. septemdierum*, *B. brevior*). It is possible, given the known long larval duration and dispersal capabilities of some Bathymodiolinae (e.g., *G. childressi* (Arellano et al., 2014; Arellano and Young, 2009)) that an ancestor of these taxa and *B. nancyschneiderae* n. sp. could have dispersed across the Pacific and/or from the Central Indian Ridge. However, due to the uncertainty of the placement of *B. nancyschneiderae* n. sp. in the phylogeny, more molecular data is needed to resolve the evolutionary origin of *B. nancyschneiderae* n. sp. While the genetic and depth separation between *B. nancyschneiderae* n. sp. and the other *Bathymodiolus* species at the Costa Rica margin is compelling, additional genetic loci will be needed to refine the placement of *B. nancyschneiderae* n. sp. in Bathymodiolinae.

Bathymodiolus thermophilus was sampled from a single seep site at the Costa Rica margin, Jaco Scar. This represents confirmation with genetic data of *B. thermophilus* at a seep environment first reported in Levin et al. (2012). *Bathymodiolus thermophilus* had previously been thought to be a vent-endemic, so its appearance at a seep is of interest. The ancestral state reconstruction of habitat for the Bathymodiolinae in this study suggests that *B. thermophilus*, which had been previously observed only at vents (Won et al., 2003; Johnson et al., 2013), may have had a seep origin (Fig. 5). The most recent common ancestor of the *Bathymodiolus* clade (excluding "*B.*" *manusensis* and "*B.*" *aduloides*) is most likely to be of seep origin as well (Fig. 5). Jaco Scar has been previously reported to have temperature anomalies of up to 3 °C above ambient seawater in areas of "shimmering water" where *B. thermophilus* mussels were sampled (Levin et al., 2012). According to Levin et al. (2012), Jaco Scar may represent an intermediate environment with both vent and seep characteristics (a "hydrothermal seep"). It is possible that intermediate environments like these facilitated the dispersal of *B. thermophilus* to both vent and seep environments, though it has not yet been reported at any of the other seep environments along the Costa Rica margin.

This study represents the first documentation of three sympatric *Bathymodiolus* species at a single dive site, Jaco Scar (as well as four species within approximately 1 km of each other). Current sampling suggests that the three newly discovered *Bathymodiolus* species are unique to this area. Other taxa that were reported at the Costa Rica margin seep sites have been reported and confirmed with genetic data at other seeps and vents north of Costa Rica, such as Vestimentifera (e.g. *Lamellibrachia barhami* (McCowin and Rouse, 2018)), Ampharetidae (e.g., *Amphisamytha fauchaldi* (Stiller et al., 2013)), Amphinomidae (e.g., *Archinome levinae* (Borda et al., 2013)), and Vesicomyidae (*Archivesica gigas* (Levin et al., 2012; Breusing et al., 2019)). However, no Bathymodiolinae have been reported at any vent sites north of 13°N on the East Pacific Rise (Johnson et al., 2013), even though surface dispersal and long duration of larval stages should make it possible for these mussels to disperse long distances (Arellano et al., 2014; Arellano and Young, 2009; Kyuno et al., 2009). Seeps are known to exist along the continental margin south of Costa Rica as far as Chile (Sellanes et al., 2008; Zapata-Hernández et al., 2014; Kobayashi and Araya, 2018), and reports of Bathymodiolinae have been made there, but little deep-sea exploration has been conducted along the coast of South America. While the dispersal capabilities of the new *Bathymodiolus* species at Costa Rica have not been directly tested, given the known dispersal capabilities of their close relatives (Arellano et al., 2014), we believe that it is likely that their range extends south of Costa Rica. Future sampling in the East Pacific, especially along the South American coast, is needed to confirm this.

4.3. Morphology and the importance of molecular data

While the molecular analyses in this study clearly revealed three new *Bathymodiolus* species from seeps at the Costa Rica margin, morphological examination did not yield this same result. Only two new species were reported in initial observations from the Costa Rica margin (Levin et al., 2012) because the four species actually present could not be differentiated morphologically (confirmed by the PCA, Fig. 10), while there was clear genetic evidence for three new mussel species and *B. thermophilus* in the molecular dataset. The disparity between the morphological and molecular data underscores the importance of molecular data for future biological and ecological studies along the Costa Rica margin. Without molecular data, the number of mussel species, the stratification of those species by depth, and the resulting evolutionary and biogeographical hypotheses for *Bathymodiolus* mussels from the Costa Rica margin would have been lost. Data like these will be important for future ecological studies and conservation efforts, which cannot hope to accurately portray ecological relationships at seeps along the Costa Rica margin without the species-level information that can only be obtained from molecular data.

5. Conclusion

This study revealed three new species of *Bathymodiolus* and confirmed the presence of *B. thermophilus* at seeps along the Costa Rica margin. While morphological data alone could not discriminate four species, molecular analyses (including phylogenies based on four mitochondrial and four nuclear genes, distance analyses, and haplotype networks) provided strong support for the three new species *B. billschneideri* n. sp., *B. earlougheri* n. sp., and *B. nancyschneiderae* n. sp., and for the presence of *B. thermophilus* at the Costa Rica margin. Our molecular analyses also revealed the depth stratification of some of the mussel species (*B. billschneideri* n. sp. restricted to deeper sites and *B. nancyschneiderae* n. sp. restricted to shallower sites).

6. Taxonomy

6.1. Family: Bathymodiolinae Kenk and Wilson, 1985.

Bathymodiolus Kenk and Wilson, 1985.
Type species: *Bathymodiolus thermophilus* Kenk and Wilson, 1985.

6.2. Bathymodiolus billschneideri n sp.

(Figs. 3 and 7; Supplementary Fig. 5A).
urn:lsid:zoobank.org:act:C0B4867B-1900-4CE9-A27F-1DD187153152
Bathymodiolus n. sp. Levin et al., (2012), p. 2583.
Bathymodiolus sp. Levin et al., (2015), supplemental data.
Bathymodiolus sp. 1 Lindgren et al., (2019), p. 153.

6.2.1. Material Examined

Holotype: SIO-BIC M12074, collected on March 7, 2009 from Jaco scar, HOV *Alvin* Dive 4513, 1817 m depth; 9.1167°N, 84.8351°W. Collected by G. Rouse and D. Huang. Subsample of foot preserved in 95% ethanol for molecular analyses; remainder of specimen fixed in 8% formalin and preserved in 50% ethanol.

Paratypes: SIO-BIC M14533 and SIO-BIC M14534 collected on May 26, 2017 from Jaco Scar, HOV *Alvin* Dive 4911, 1891 m depth; 9.1151°N, 84.8468°W. Subsample of foot preserved in 95% ethanol, 1 valve cleaned for dry preservation. SIO-BIC M16763 and SIO-BIC M16793 collected on October 18, 2018 from Jaco Scar, HOV *Alvin* Dive 4972, 1784 m depth; 9.1178°N, 84.8395°W. Subsample of foot preserved in 95% ethanol, 1 valve cleaned for dry preservation. SIO-BIC M17000 collected on November 5, 2018 from Parrita Seep, HOV Alvin Dive 4990, 1400 m depth; 9.0318°N, 84.6205°W. Subsample of foot preserved in 95% ethanol, 1 valve cleaned for dry preservation. MZUCR 8578 collected on March 3, 2009 from Jaco Scar, HOV *Alvin* Dive 4509, 1783 m depth; 9.1172°N, 84.8417°W. Subsample of foot preserved in 95% ethanol for molecular analyses; remainder of specimen fixed in 8% formalin and preserved in 50% ethanol.

Other Material Examined: See Table 1 and Supplementary Table 1 for genetic data and Supplementary Table 3 for additional morphological data.

6.2.2. Description

Shell large, up to 189.14 mm (Supplementary Table 3), thin but sturdy, elongate modioliform, equivalve, slightly variable in outline. Shell height to length ratio 0.35–0.56, width to length ratio 0.12–0.24. Shell height gradually increasing anteriorly, curved dorsoventrally, most inflated at the middle, with a broadly rounded ridge extending from umbonal region to posterior-ventral margin. Anterior margin short and narrow but evenly rounded; ventral margin slightly concave. Posterior margin broadly rounded; posterio-dorsal angulation well defined, broadly rounded, situated anteriorly to the posterior adductor scar. Dorsal margin markedly convex, slightly curved to straight over the span of the ligament, highest part of the valve situated along middle of ligament. Umbones fairly narrow and flattened, situated 5–10% posteriorly from anterior margin, subterminal, prosogyrate; eroded with nacreous layer free in larger specimens (Fig. 7).

Ligament plate narrow, slightly convex to straight. Exterior smooth except for well-developed, irregular commarginal growth lines and very faint and irregularly spaced radial striae in periostracum running from the umbo to the posterior/dorsal margin. Periostracum smooth, glossy, thick and yellow to brown, lightest in umbonal and posterior margin regions, darkest on anterior-dorsal slope, curving over shell edge. Byssal hairs and byssal endplates of other specimens often scattered over surface. Shell dull-white to grey under periostracum (Fig. 7). Ligament opisthodetic, long and narrow, extending over four-fifths to five-sixth of the

Postero-dorsal margin in front of the postero-dorsal corner, ending posteriorly with a slight taper. Hinge edentulous, hinge thickened below and anterior to umbo. Hinge denticles absent in smallest specimens.

Anterior adductor scar small and rounded but truncated posteriorly, situated medially/dorsally in the anterior part of the valve, partly below and partially anterior to umbo, distant to antero-ventral margin. Anterior byssal-pedal retractor scar oval, located high within umbonal cavity behind umbo. Posterior adductor scar rounded-rectangular. Posterior byssal-pedal retractor muscles form two separate scars with large gap between them, anterior one elongate-elliptical, located high, and close to posterior end of ligament, second one elliptical and located antero-dorsally to but contiguous with posterior adductor scar to form a joint comma-shaped scar. Pallial line distinct, extending ventrally from anterior adductor to posterior adductor, parallel to ventral margin (Supplementary Fig. 5A).

Animal with long, narrow ctenida, 100 mm long and 11 mm broad in holotype; outer demibranchs anteriorly slightly shorter than inner demibranch; both demibranchs end abruptly anteriorly, taper posteriorly (Fig. 7B). Filaments broad and fleshy, ventral edges lack food grooves. Foot medium sized, 27 mm long (byssus orifice included) in holotype. Foot thick, flattened, slightly terminally swollen; byssal groove running along ventral surface almost to tip. Byssal threads sparce, usually emerging as separate strands from orifice, strands thick and strong. Foot-byssus retractor complex moderately prolongated like the shell. Posterior byssal retractors in two roughly equal main bundles arising together at base of byssus but diverge and attach separately to shell. Posterior pedal retractors thick, arising from base of foot anterior to origin of posterior byssal retractors, passing dorsally on both inner and outer sides of most anterior bundles of posterior retractors (Fig. 7B).

6.2.3. Etymology

This species is named for William (Bill) Schneider, a San Diego native and lover of all marine life including molluscs, and a great supporter of the Benthic Invertebrate Collection at Scripps Institution of Oceanography.

6.2.4. Distribution

Bathymodiolus billschneideri n. sp. is known from Jaco Scar (1783–1891 m) and Parrita Seep (1400 m).

6.2.5. Variation

Bathymodiolus billschneideri n. sp. specimens differ genetically by at most a few base pairs (COI, Fig. 3); there is considerable color variation between specimens, from dark brown to gold and yellow (Fig. 7E–F).

6.2.6. Remarks

The shells of *Bathymodiolus billschneideri* n. sp. most closely resemble those of *B. nancyschneiderae* n. sp., with the PCA unable to separate the two species morphologically (Supplemental Fig. 5). Overall size ranges, umbone location, ligament length, and muscle scars of the two species were also very similar. The two species are separated by approximately 400–800 m, with *B. billschneideri* n. sp. occurring at depths of approximately 1400–1800 m and *B. nancyschneiderae* n. sp. occurring at depths

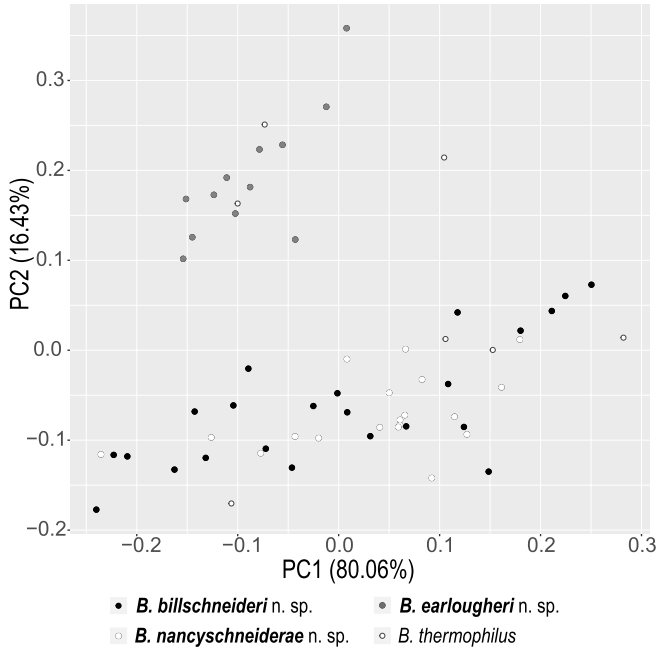

Fig. 10. Principal component analysis of shell length, shell width, and shell height of *Bathymodiolus billschneideri* n. sp., *B. earlougheri* n. sp., *B. nancyschneiderae* n. sp., and *B. thermophilus*.

of approximately 1000–1100 m. *Bathymodiolus billschneideri* n. sp. is often slightly lighter in coloration than *B. nancyschneiderae* n. sp., has a less angular postero-dorsal corner, a wider posterior part, and a more evenly concave ventral margin. The shell of *B. billschneideri* n. sp. also resembles *B. thermophilus*. The two species can sometimes be differentiated by color: the darker brown specimens of *B. billschneideri* n. sp. can be differentiated from the golden-yellow *B. thermophilus* (Figs. 6 and 7). However, the yellow *B. billschneideri* n. sp. specimens could not be differentiated from *B. thermophilus* specimens from Costa Rica (Fig. 6A–B, 7), but tended to have a more elongate shell shape that allowed them to be differentiated from *B. thermophilus* specimens from the East Pacific Rise (Fig. 6C–D, 7).

6.3. *Bathymodiolus earlougheri n sp.*

(Figs. 3 and 8; Supplementary Fig. 5B).

urn:lsid:zoobank.org:act:CDD83187-F83C-4FAE-A730-026A3C3EC989

Bathymodiolus sp. Aguado and Rouse (2011), p. 114.

Bathymodiolus n. sp. Levin et al., (2012), p. 2583.

Bathymodiolus sp. Levin et al., (2015), supplemental data.

Bathymodiolus sp. 3 Lindgren et al., (2019), p. 153.

6.3.1. *Material Examined*

Holotype: SIO-BIC M12076 collected on March 7, 2009 from Jaco Scar, HOV *Alvin* Dive 4513, 1817m depth; 9.1167°N, 84.8351°W. Collected by G. Rouse and D. Huang. Subsample of foot preserved in 95% ethanol for molecular analyses; remainder of specimen fixed in 8% formalin and preserved in 50% ethanol.

Paratypes: SIO-BIC M12080 collected on March 7, 2009 from Jaco Scar, HOV *Alvin* Dive 4513, 1817 m depth; 9.1167°N, 84.8351°W. Subsample of foot preserved in 95% ethanol, 1 valve cleaned for dry preservation. SIO-BIC M14479 collected on May 22, 2017 from Mound 12, HOV *Alvin* Dive 4907, 999 m depth; 8.9304°N, 84.3128°W. Subsample of foot preserved in 95% ethanol, 1 valve cleaned for dry preservation. MZUCR 8579 collected on March 7, 2009 from Jaco Scar, HOV *Alvin* Dive 4513, 1817 m depth; 9.1167°N, 84.8351°W. Subsample of foot preserved in 95% ethanol for molecular analyses; remainder of specimen fixed in 8% formalin and preserved in 50% ethanol.

Other Material Examined: See Table 1 and Supplementary Table 1 for genetic data and Supplementary Table 3 for additional morphological data.

6.3.2. *Description*

Shell medium sized, up to 119.9 mm, short and stout modioliform, thin but fairly sturdy, equivalve, very inflated, elliptical in immature specimens, becoming increasingly arculate in larger, older specimens. Shell height to length ratio 0.44–0.56, shell width to height ratio 0.2–0.24. Shell height increasing posteriorly, exhibiting somewhat trapezoid outline. Anterior margin narrowly rounded, posterior margin broadly rounded, ventral margin straight to very slightly concave. Dorsal margin convex, postero-dorsal corner indistinct and gently rounded. Umbones prosogyrate low, broad and flattened, subterminal to nearly terminal in some specimens, situated 3–7% posteriorly from anterior margin, eroded in larger specimens with nacreous layer free. An indistinct, raised, and broadly rounded ridge extends from the umbonal region to the postero-ventral margin (Fig. 8).

Exterior smooth except for faint, irregular commarginal growth lines. Periostracum smooth, dull to somewhat glossy, thin and golden brown to copper brown to golden, occasionally byssal endplates and hair present from other specimens. Shell dull-white under periostracum. Ligament plate narrow, slightly convex to straight. Ligament opisthodetic, extending posteriorly from umbones to occupy ~40% of dorsal margin. Posterior end of ligament tapering, subligamental shell ridge strong and angular. Adult hinge edentulous, thickened below and anterior to umbo (Fig. 8).

Muscle scars and pallial line fairly indistinct. Anterior adductor muscle scar small and oblong, tapering posteriorly, situated more ventrally in the anterior part of the valve, partly below and partially posterior to umbo. Posterior adductor scar round, contiguous dorsaly with single posterior byssal-pedal retractor scar; posterior byssal retractors forming continuous scar extending from directly beneath posterior end of ligament to antero-dorsal edge of posterior adductor scar. Ventral pallial line straight, paralleling the ventral shell margin and extending from postero-ventral edge of anterior adductor scar to posterior adductor (Supplementary Fig. 5B).

Animal with long, wide ctenida, 86 mm long and 7 mm broad in holotype; outer demibranchs anteriorly slightly shorter than inner demibranch; both demibranchs end abruptly anteriorly (Fig. 8D). Filaments broad and fleshy, ventral edges lack food grooves. Foot small sized, 13 mm long (byssus orifice included) in holotype. Foot fairly thick, rounded, terminally tapered; byssal groove running along ventral surface almost to tip. Byssus sparse, usually emerging as separate strands from orifice, strands thick and strong. Foot-byssus retractor complex moderately prolongated like the shell. Posterior byssal retractors in two roughly equal main bundles arising together at base of byssus but diverge and attach separately to shell. Posterior pedal retractors thick, arising from base of foot anterior to origin of posterior byssal retractors, passing dorsally on both inner and outer sides of most anterior bundles of posterior retractors (Fig. 8).

6.3.3. *Etymology*

This species is named in memory of Robert Charles “Chuck” Earlougher in recognition of the support of the SIO Collections by his daughter Jan and her husband Jim Hawkins.

6.3.4. *Distribution*

Bathymodiolus earlougheri n. sp. is known from Jaco Scar (1812–1891 m), The Thumb (1073 m), and Mound 12 (999–1008 m).

6.3.5. *Variation*

Bathymodiolus earlougheri n. sp. specimens differ genetically by at most a few base pairs (COI, Fig. 3) and show less morphological

variation in shell color and shape than *B. billschneideri* n. sp. specimens (Fig. 8).

6.3.6. Remarks

Bathymodiolus earlougheri n. sp. morphologically resembles *B. azoricus* and B. *thermophilus* (East Pacific Rise specimens). *Bathymodiolus earlougheri* n. sp. is stouter, wider, more wedge shaped, and lighter and more golden in color than *B. azoricus*. *Bathymodiolus earlougheri* n. sp. shells also closely resemble *B. thermophilus* specimens that are under ~10 cm long, sharing a similar wedge modioliform shape and straight to slightly concave ventral margin. However, the umbones are more anteriorly situated in *B. earlougheri* n. sp., and larger specimens are more elongate with a concave ventral margin and therefore easily distinguishable. *Bathymodiolus earlougheri* n. sp. also shares the two-bundle foot byssus retractor complex with *B. thermophilus*. *Bathymodiolus earlougheri* n. sp. is easily morphologically distinguishable from the two other new seep species, *B. billschneideri* n. sp. and *B. nancyschneiderae* n. sp., by its golden color and compact shape (Figs. 8 and 10).

6.4. *Bathymodiolus nancyschneiderae n sp.*

(Figs. 3 and 9; Supplementaary Fig. 5C).

urn:lsid:zoobank.org:act:FCC9AAEF-BCD6-48DB-85F8-3069C95DFE20

Bathymodiolus n. sp. Levin et al., (2012), p. 2583.

Bathymodiolus sp. Levin et al., (2015), supplemental data.

Bathymodiolus sp. 2 Lindgren et al., (2019), p. 153.

6.4.1. Material Examined

Holotype: SIO-BIC M12032, collected on March 3, 2009 from Jaco-1000, HOV *Alvin* Dive 4509, 1063 m depth; 9.1172°N, 84.8417°W. Collected by G. Rouse and D. Huang. Subsample of foot preserved in 95% ethanol for molecular analyses; remainder of specimen fixed in 8% formalin and preserved in 50% ethanol.

Paratypes: SIO-BIC M14530 and SIO-BIC M14531 collected on May 24, 2017 from Mound 12, HOV Alvin Dive 4909, 1000 m depth; 8.9305°N, 84.3125°W. Subsample of foot preserved in 95% ethanol, 1 valve cleaned for dry preservation. SIO-BIC M16778 collected on October 21, 2018 from Mound 12, HOV *Alvin* Dive 4975, 1000 m depth; 8.9337°N, 84.3067°W. Subsample of foot preserved in 95% ethanol, 1 valve cleaned for dry preservation. MZUCR 8577 collected on March 3, 2009 from Jaco-1000, HOV *Alvin* Dive 4509, 1063 m depth; 9.1172°N, 84.8417°W. Fixed in 8% formalin and preserved in 50% ethanol.

Other Material Examined: See Table 1 and Supplementary Table 1 for genetic data and Supplementary Table 3 for additional morphological data.

6.4.2. Description

Shell large up to 181.67 mm, thick sturdy, elongate modioliform, equivalve, slightly variable in outline. Shell height to length ratio 0.37–0.42, shell width to shell length ratio 0.13–0.15. Shell height gradually increasing anteriorly, curved dorsoventrally, most inflated at the middle, with a broadly rounded ridge extending from umbonal region to postero-ventral margin. Anterior margin short and narrow but evenly rounded; ventral margin markedly concave, with most concave part located far anteriorly. Posterior margin broadly rounded; posterio-dorsal angulation ill-defined, very broadly rounded, situated anteriorly to the posterior adductor scar. Dorsal margin markedly convex, slightly curved to straight over the span of the ligament, highest part of the valve situated along middle of ligament. Umbones fairly narrow and flattened, situated 9–13% posteriorly from anterior margin, subterminal, prosogyrate; eroded with nacreous layer free in larger specimens (Fig. 9).

Ligament plate narrow, slightly convex to straight. Exterior smooth except for well-developed, irregular commarginal growth lines and very faint and irregularly spaced radial striae in periostracum running from the umbo to the posterior/dorsal margin. Periostracum smooth, glossy, thick and brown to dark brown, lightest in umbonal and posterior margin regions, darkest on anterior-dorsal slope, curving over shell edge. Byssal hairs and byssal endplates of other specimens often scattered over the surface, polychaete tubes often present. Shell dull-white to grey under periostracum (Fig. 9). Ligament opisthodetic, long and narrow, extending over ~80% of the postero-dorsal margin in front of the postero-dorsal corner, ending posteriorly with a slight taper. Hinge edentulous in large specimens, hinge thickened below and anterior to umbo. Hinge denticles absent in smallest specimens.

Anterior adductor scar medium and rounded, situated medially/dorsally in the anterior part of the valve, partly below and partially anterior to umbo, distant to antero-dorsal margin. Anterior byssal-pedal retractor scar elliptical, located within umbonal cavity behind umbo; posterior adductor scar rounded and elongate; posterior byssal-pedal retractor muscles form two separate scars with gap between them, anterior one elongate-elliptical, located high, and close to posterior end of ligament, second one elliptical and located antero-dorsally to but contiguous with posterior adductor scar to form a joint comma-shaped scar. Pallial line distinct, extending ventrally from anterior adductor to posterior adductor, parallel to ventral margin (Supplementary Fig. 5C).

Animal with long, narrow ctenida, 138 mm long and 12 mm broad in holotype; outer demibranchs anteriorly slightly shorter than inner demibranch; both demibranchs end abruptly anteriorly. Filaments broad and fleshy, ventral edges lack food grooves. Foot medium sized, 24 mm long (byssus orifice included) in holotype. Foot thick, rounded, terminally tapered; byssal groove running along ventral surface almost to tip. Byssus abundant, usually emerging as separate strands from orifice, strands dark, thick and strong. Foot-byssus retractor complex moderately prolongated like the shell. Posterior byssal retractors in two roughly equal main bundles arising together at base of byssus but diverge and attach separately to shell. Posterior pedal retractors thick, arising from base of foot anterior to origin of posterior byssal retractors, passing dorsally on both inner and outer sides of most anterior bundles of posterior retractors (Fig. 9).

6.4.3. Etymology

This species is named for Nancy Schneider, a San Diego native and lover of all marine life including molluscs, and a great supporter of the Benthic Invertebrate Collection at Scripps Institution of Oceanography.

6.4.4. Distribution

Bathymodiolus nancyschneiderae n. sp. is known from Mound 12 (999–1008 m), Jaco-1000 (1063 m), and The Thumb (1072–1073 m).

6.4.5. Variation

Bathymodiolus nancyschneiderae n. sp. specimens differ genetically by at most a few base pairs (COI, Fig. 3) and tend to have less color variation than *B. billschneideri* n. sp. specimens. However, some smaller *B. nancyschneiderae* n. sp. specimens have a more golden-brown color (similar to *B. billschneideri* n. sp.) than the larger adults (Fig. 9E–F).

6.4.6. Remarks

The shell of *B. nancyschneiderae* n. sp. most closely resembles that of *B. billschneideri* n. sp., with the PCA unable to separate the two species morphologically (Fig. 10). Overall size ranges, umbone location, ligament length, and muscle scars of the two species are also very similar. The two species do not co-occur at a single dive site but are found at different depths within 1 km of each other (Jaco-1000 and Jaco Scar, approximately 1000 m and 1800 m, respectively). *Bathymodiolus nancyschneiderae* n. sp. tends to have a darker periostracum than *B. billschneideri* n. sp., and a rounder and wider postero-dorsal corner, a narrower posterior part, and the most concave part of the ventral margin is not in the middle of the shell as in *B. billschneideri* n. sp. but more anteriorly situated. The shell of *B. nancyschneiderae* n. sp. also resembles

B. azoricus, *B. brooksi*, and *B. heckerae*. It is distinguished from *B. azoricus* by a markedly more concave ventral margin, more pronounced umbones, and a more elongate form. Both *B. heckerae* and *B. brooksi* have the same periostracal coloration as *B. nancyschneiderae* n. sp., but both have a straighter ventral margin, more posteriorly situated umbones, and a more posteriorly situated postero-dorsal corner.

Declaration of competing interest

The authors declare that they have no known competing financial interests or personal relationships that could have appeared to influence the work reported in this paper.

Acknowledgements

Many thanks to Chief Scientists Lisa Levin and Erik Cordes, the captain and crew of the *R/V Atlantis* and the *R/V Falkor*, and the pilots of the HOV *Alvin* and ROV *SuBastian* for crucial assistance in specimen collection on cruises to Costa Rica. Thanks also to Charlotte Seid for collection management at SIO-BIC. We would also like to thank Shirley Sorokin and the South Australian Museum (SAM) for curation of samples. We thank Bill and Nancy Schneider and Jan and Jim Hawkins for their support of the SIO Collections and the Schmidt Ocean Institute for ship time support and publishing costs. This project was supported by the US National Science Foundation (NSF OCE-0826254, OCE-0939557, OCE-1634172).

Appendix A. Supplementary data

Supplementary data to this article can be found online at https://doi.org/10.1016/j.dsr.2020.103322.

References

Aguado, M.T., Rouse, G.W., 2011. Nautiliniellidae (Annelida) from costa rican cold seeps and a western pacific hydrothermal vent, with description of four new species. Syst. Biodivers. 9, 109–131. https://doi.org/10.1080/14772000.2011.569033.

Arellano, S.M., Van Gaest, A.L., Johnson, S.B., Vrijenhoek, R.C., Youn, C.M., 2014. Larvae from deep-sea methane seeps disperse in surface waters. Proc. R. Soc. B Biol. Sci. 281, 8. https://doi.org/10.1098/rspb.2013.3276.

Arellano, S.M., Young, C.M., 2009. Spawning, development, and the duration of larval life in a deep-sea cold-seep mussel. Biol. Bull. 216, 149–162. https://doi.org/10.2307/25470737.

Audzijonyte, A., Vrijenhoek, R.C., 2010. Three nuclear genes for phylogenetic, SNP and population genetic studies of molluscs and other invertebrates. Mol. Ecol. Resour. 10, 200–204. https://doi.org/10.1111/j.1755-0998.2009.02737.x.

Baco-Taylor, A.R., 2002. Food-web structure, succession and phylogenetics on deep-sea whale skeletons. PhD Thesis. The University of Hawaii.

Bandelt, H., Forster, P., Röhl, A., 1999. Median-joining networks for inferring intraspecific phylogenies. Mol. Biol. Evol. 16, 37–48.

Bazin, E., Glemin, S., Galtier, N., 2006. Population size does not influence mitochondrial genetic diversity in animals. Science 84 312, 570–572. https://doi.org/10.1126/science.1122033.

Borda, E., Kudenov, J.D., Chevaldonne, P., Blake, J.A., Desbruyeres, D., Fabri, M.-C., Hourdez, S., Pleijel, F., Shank, T.M., Wilson, N.G., Schulze, A., Rouse, G.W., 2013. Cryptic species of *Archinome* (Annelida: amphinomida) from vents and seeps. Proc. R. Soc. B Biol. Sci. 280, 9. https://doi.org/10.1098/rspb.2013.1876.

Bouckaert, R., Vaughan, T.G., Barido-Sottani, J., Duchêne, S., Fourment, M., Gavryushkina, A., Heled, J., Jones, G., Kühnert, D., De Maio, N., Matschiner, M., Mendes, F.K., Müller, N.F., Ogilvie, H.A., du Plessis, L., Popinga, A., Rambaut, A., Rasmussen, D., Siveroni, I., Suchard, M.A., Wu, C.H., Xie, D., Zhang, C., Stadler, T., Drummond, A.J., 2019. Beast 2.5: an advanced software platform for Bayesian evolutionary analysis. PLoS Comput. Biol. 15 (4), 28. https://doi.org/10.1371/journal.pcbi.1006650 e1006650.

Breton, S., Beaupré, H.D., Stewart, D.T., Hoeh, W.R., Blier, P.U., 2007. The unusual system of doubly uniparental inheritance of mtDNA: isn't one enough? Trends Genet. 23, 465–474. https://doi.org/10.1016/j.tig.2007.05.011.

Breusing, C., Johnson, S.B., Vrijenhoek, R.C., Young, C.R., 2019. Host hybridization as a potential mechanism of lateral symbiont transfer in deep-sea vesicomyid clams. Mol. Ecol. 1–12. https://doi.org/10.1111/mec.15224.

Catresana, J., 2000. Selection of conserved blocks from multiple alignments for their use in phylogenetic analysis. Mol. Biol. Evol. 17, 540–522.

Chernomor, O., Von Haeseler, A., Minh, B.Q., 2016. Terrace aware data structure for phylogenomic inference from supermatrices. Syst. Biol. 65, 997–1008. https://doi.org/10.1093/sysbio/syw037.

Colgan, D.J., McLauchlan, A., Wilson, G.D.F., Livingston, S.P., Edgecombe, G.D., Macaranas, J., Cassis, G., Gray, M.R., 1998. Histone H3 and U2 snRNA DNA sequences and arthropod molecular evolution. Aust. J. Zool. 46 (5), 419–437. https://doi.org/10.1071/ZO98048.

Cosel, R. von, Comtet, T., Krylova, E.M., 1999. *Bathymodiolus* (Bivalvia: Mytilidae) from hydrothermal vents on the Azores triple junction and the Logatchev hydrothermal field. Veliger 42, 218–248.

Cosel, R. von, Marshall, B.A., 2010. A new genus and species of large mussel (Mollusca: Bivalvia: Mytilidae) from the Kermadec Ridge. TUHINGA 21, 59–73.

Cosel, R. Von, Marshall, B.A., 2003. Two new species of large mussels (Bivalvia: Mytilidae) from active submarine volcanoes and a cold seep off the eastern North Island of New Zealand, with description of a new genus. Nautilus 117, 31–46.

Cosel, R. von, Olu, K., 1998. Gigantism in Mytilidae: a new *Bathymodiolus* from cold seeps on the Barbados accretionary prism. Comptes-Rendus de l'Académie des Sciences, ser. 3. Sci. la Vie 321, 655–663.

Dall, W.H., Bartsch, P., Rehder, H.A., 1938. A manual of the recent and fossil marine pelecypod mollusks of the Hawaiian Islands. Bish. Museum Bull. 153, 233.

Darriba, D., Taboada, G.L., Doallo, R., Posada, D., 2012. jModelTest 2: more models, new heuristics and parallel computing. Nat. Methods 9. https://doi.org/10.1038/nmeth.2109, 772–772.

Dautzenberg, P., 1927. Mollusques provenant des campagnes scientifiques du Prince Albert Ier de Monaco dans l'Océan Atlantique et dans le Golfe de Gascogne. Résultats des Campagnes Sci. Accompl. sur son Yacht par Albert Ier Prince Souver. Monaco 72, 401.

Dell, R.K., 1987. Mollusca of the family Mytilidae (Bivalvia) associated with organic remains from deep water off New Zealand, with revisions of the genera *Adipicola* Dautzenberg, 1927 and *Idasola* Iredale, 1915. Natl. Museum New Zeal. Rec. 3, 17–36.

Distel, D.L., Baco, A.R., Chuang, E., Morrill, W., Cavanaugh, C., Smith, C.R., 2000. Do mussels take wooden steps to deep-sea vents? Nature 403, 725–726.

Duperron, S., Halary, S., Lorion, J., Sibuet, M., Gaill, F., 2008. Unexpected co-occurrence of six bacterial symbionts in the gills of the cold seep mussel *Idas* sp. (Bivalvia: Mytilidae). Environ. Microbiol. 10, 433–445. https://doi.org/10.1111/j.1462-2920.2007.01465.x.

Fisher, C.R., Brooks, J.M., Vodenichar, J.S., Zande, J.M., Childress, J.J., Burke Jr., R.A., 1993. The co-occurrence of methanotrophic and chemoautotrophic sulfur-oxidizing bacterial symbionts in a deep-sea mussel. Mar. Ecol. 14, 277–289. https://doi.org/10.1111/j.1439-0485.1993.tb00001.x.

Fujita, Y., Matsumoto, H., Fujiwara, Y., Hashimoto, J., Galkin, S.V., Ueshima, R., Miyazaki, J.-I., 2009. Phylogenetic relationships of deep-sea *Bathymodiolus* mussels to their Mytilid relatives from sunken whale carcasses and wood. Venus 67, 123–134.

Giribet, G., Carranza, S., Baguna, J., Riutort, M., Ribera, C., 1996. First molecular evidence for the existence of a Tardigrada plus Arthropoda clade. Mol. Biol. Evol. 13 (1), 76–84. https://doi.org/10.1093/oxfordjournals.molbev.a025573.

Govenar, B., 2010. Shaping vent and seep communities: habitat provision and modification by foundation species. In: Kiel, S. (Ed.), The Vent and Seep Biota: Aspects from Microbes to Ecosystems. Springer, pp. 403–432. https://doi.org/10.1007/978-90-481-9572-5.

Guindon, S., Gascuel, O., 2003. A simple, fast and accurate method to estimate large phylogenies by maximum-likelihood. Syst. Biol. 52, 696–704.

Gustafson, R.G., Turner, R.D., Lutz, R.A., Vrijenhoek, R.C., 1998. A new genus and five new species of mussels (Bivalvia: Mytilidae) from deep-sea sulfide/hydrocarbon seeps in the Gulf of Mexico. Malacologia 40, 63–112.

Hasegawa, M., Kishino, H., Yano, T. aki, 1985. Dating of the human-ape splitting by a molecular clock of mitochondrial DNA. J. Mol. Evol. 22, 160–174. https://doi.org/10.1007/BF02101694.

Hashimoto, J., 2001. A new species of *Bathymodiolus* (Bivalvia: Mytilidae) from hydrothermal vent communities in the Indian Ocean. Venus 60, 141–149.

Hashimoto, J., Furuta, M., 2007. A new species of *Bathymodiolus* (Bivalvia: Mytilidae) from hydrothermal vent communities in the Manus Basin, Papua New Guinea. Venus 66, 57–68.

Iwasaki, H., Kyuno, A., Shintaku, M., Fujita, Y., Fujiwara, Y., Fujikura, K., Hashimoto, J., Martins, L. de O., Gebruk, A., Miyazaki, J.-I., 2006. Evolutionary relationships of deep-sea mussels inferred by mitochondrial DNA sequences. Mar. Biol. 149, 1111–1122. https://doi.org/10.1007/s00227-006-0268-6.

Jeffreys, J.G., 1876. New and peculiar Mollusca of the Pecten, Mytilus and Arca families, procured in the Valorous expedition. Ann. Mag. Nat. Hist. 18, 424–436.

Johnson, S.B., Won, Y.-J., Harvey, J.B., Vrijenhoek, R.C., 2013. A hybrid zone between *Bathymodiolus* mussel lineages from eastern Pacific hydrothermal vents. BMC Evol. Biol. 13, 18. https://doi.org/10.1186/1471-2148-13-21.

Jones, W.J., Won, Y.-J., Maas, P.A.Y., Smith, P.J., Lutz, R.A., Vrijenhoek, R.C., 2006. Evolution of habitat use by deep-sea mussels. Mar. Biol. 148, 841–851. https://doi.org/10.1007/s00227-005-0115-1.

Jovelin, R., Justine, J.-L., 2001. Phylogenetic relationships within the polyopisthocotylean monogeneans (Platyhelminthes) inferred from partial 28S rDNA sequences. Int. J. Parasitol. 31 (4), 393–401. https://doi.org/10.1016/S0020-7519(01)00114-X.

Kassambara, A., Mundt, F., 2019. Factoextra: Extract and Visualize the Results of Multivariate Data Analyses.

Katoh, K., Standley, D.M., 2013. MAFFT multiple sequence alignment software version 7: improvements in performance and usability. Mol. Biol. Evol. 30, 772–780. https://doi.org/10.1093/molbev/mst010.

Kenk, V.C., Wilson, B.R., 1985. A new mussel (Bivalvia, Mytilidae) from hydrothermal vents in the Galapagos rift zone. Malacologia 26, 253–271.

Kiel, S. (Ed.), 2010. The Vent and Seep Biota: Aspects from Microbes to Ecosystems. Springer. https://doi.org/10.1007/978-90-481-9572-5.
Kiel, S., Little, C.T.S., 2006. Cold-seep mollusks are older than the general marine mollusk fauna. Science 313 (5792), 1429–1431. https://doi.org/10.1126/science.1126286.
Kobayashi, G., Araya, J.F., 2018. Southernmost records of *Escarpia spicata* and *Lamellibrachia barhami* (Annelida: siboglinidae) confirmed with DNA obtained from dried tubes collected from undiscovered reducing environments in northern Chile. PloS One 13 (10), 1–13. https://doi.org/10.1371/journal.pone.0204959 e0204959.
Krylova, E., Sahling, H., Janssen, R., 2010. *Abyssogena*: a new genus of the family Vesicomyidae (Bivalvia) from deep water vents and seeps. J. Molluscan Stud. 76, 107–132.
Kyuno, A., Shintaku, M., Fujita, Y., Matsumoto, H., Utsumi, M., Watanabe, H., Fujiwara, Y., Miyazaki, J.-I., 2009. Dispersal and differentiation of deep-sea mussels of the genus *Bathymodiolus* (Mytilidae, Bathymodiolinae). J. Mar. Biol. 15. https://doi.org/10.1155/2009/625672, 2009.
LaBella, A.L., Van Dover, C.L., Jollivet, D., Cunningham, C.W., 2017. Gene flow between Atlantic and Pacific Ocean basins in three lineages of deep-sea clams (Bivalvia: Vesicomyidae: Pliocardiinae) and subsequent limited gene flow within the Atlantic. Deep. Res. Part II Top. Stud. Oceanogr. 137, 307–317. https://doi.org/10.1016/j.dsr2.2016.08.013.
Le, S., Josse, J., Husson, F., 2008. FactoMineR: an R package for multivariate analysis. J. Stat. Software 25, 1–18. https://doi.org/10.18637/jss.v025.i01.
Leigh, J., Bryant, D., 2015. PopART: full-feature software for haplotype network construction. Methods Ecol. Evol. 6, 1110–1116.
Levin, L.A., Mendoza, G.F., Grupe, B.M., Gonzalez, J.P., Jellison, B., Rouse, G., Thurber, A.R., Waren, A., 2015. Biodiversity on the rocks: macrofauna inhabiting authigenic carbonate at Costa Rica methane seeps. PloS One 10 (7), e0131080. https://doi.org/10.1371/journal.pone.0131080.
Levin, L.A., Orphan, V.J., Rouse, G.W., Rathburn, A.E., Ussler, W., Cook, G.S., Goffredi, S. K., Perez, E.M., Waren, A., Grupe, B.M., Chadwick, G., Strickrott, B., 2012. A hydrothermal seep on the Costa Rica margin: middle ground in a continuum of reducing ecosystems. Proc. R. Soc. B Biol. Sci. 279, 2580–2588. https://doi.org/10.1098/rspb.2012.0205.
Lindgren, J., Hiley, A.S., Hourdez, S., Rouse, G.W., 2019. Phylogeny and biogeography of *Branchipolynoe* (Polynoidae, Phyllodocida, Aciculata, Annelida), with descriptions of five new species from methane seeps and hydrothermal vents. Diversity 11, 153.
Lorion, J., Buge, B., Cruaud, C., Samadi, S., 2010. New insights into diversity and evolution of deep-sea Mytilidae (Mollusca: Bivalvia). Mol. Phylogenet. Evol. 57, 71–83. https://doi.org/10.1016/j.ympev.2010.05.027.
Lorion, J., Duperron, S., Gros, O., Cruaud, C., Samadi, S., 2009. Several deep-sea mussels and their associated symbionts are able to live both on wood and on whale falls. Proc. R. Soc. B Biol. Sci. 276, 177–185. https://doi.org/10.1098/rspb.2008.1101.
Lorion, J., Kiel, S., Faure, B., Kawato, M., Ho, S.Y.W., Marshall, B., Tsuchida, S., Miyazaki, J.-I., Fujiwara, Y., 2013. Adaptive radiation of chemosymbiotic deep-sea mussels. Proc. R. Soc. B Biol. Sci. 280 (1770), 20131243. https://doi.org/10.1098/rspb.2013.1243, 10.
Maas, Paula A.Y., O'Mullan, Gregory D., Lutz, Richard A., Vrijenhoek, Robert C., 1999. Genetic and morphometric characterization of mussels (Bivalvia: Mytilidae) from Mid-Atlantic hydrothermal vents. Biol. Bull. 196, 265–272. https://doi.org/10.2307/1542951.
Maddison, W.P., Maddison, D.R., 2018. Mesquite: a modular system for evolutionary analysis. Version 3.51. http://www.mesquiteproject.org.
McCowin, M.F., Rouse, G.W., 2018. A new *Lamellibrachia* species and confirmed range extension for *Lamellibrachia barhami* (Siboglinidae, Annelida) from Costa Rica methane seeps. Zootaxa 4504, 1–22. https://doi.org/10.11646/zootaxa.4504.1.1.
Miller, M.A., Pfeiffer, W., Schwartz, T., 2010. Creating the CIPRES Science Gateway for inference of large phylogenetic trees. In: Proceedings of the Gateway Computing Environments Workshop (GCE). New Orleans, LA, pp. 1–8.
Miyazaki, J.-I., Martins, L. de O., Fujita, Y., Matsumoto, H., Fujiwara, Y., 2010. Evolutionary process of deep-sea *Bathymodiolus* mussels. PloS One 5 (4), 11. https://doi.org/10.1371/journal.pone.0010363 e10363.
Miyazaki, J.-I., Shintaku, M., Kyuno, A., Fujiwara, Y., Hashimoto, J., Iwasaki, H., 2004. Phylogenetic relationships of deep-sea mussels of the genus *Bathymodiolus* (Bivalvia: Mytilidae). Mar. Biol. 144 (3), 527–535. https://doi.org/10.1007/s00227-003-1208-3.
O'Dea, A., Lessios, H.A., Coates, A.G., Eytan, R.I., Restrepo-moreno, S.A., Cione, A.L., Collins, L.S., Queiroz, A. De, Farris, D.W., Norris, R.D., Stallard, R.F., Woodburne, M. O., Aguilera, O., Aubry, M., Berggren, W.A., Budd, A.F., Cozzuol, M.A., Coppard, S. E., Duque-caro, H., Finnegan, S., Gasparini, G.M., Grossman, E.L., Johnson, K.G., Keigwin, L.D., Knowlton, N., Leigh, E.G., Leonard-pingel, J.S., Marko, P.B., Pyenson, N.D., Rachello-dolmen, P.G., Soibelzon, E., Soibelzon, L., Todd, J.A., Vermeij, G.J., Jackson, J.B.C., 2016. Formation of the Isthmus of Panama. Sci. Adv. 2, 11. https://doi.org/10.1126/sciadv.1600883.
Olu-Le Roy, K., Cosel, R. von, Hourdez, S., Carney, S.L., Jollivet, D., 2007. Amphi-Atlantic cold-seep *Bathymodiolus* species complexes across the equatorial belt. Deep. Res. Part I Oceanogr. Res. Pap. 54, 1890–1911. https://doi.org/10.1016/j.dsr.2007.07.004.
Passamonti, M., Ricci, A., Milani, L., Ghiselli, F., 2011. Mitochondrial genomes and doubly uniparental inheritance: new insights from *Musculista senhousia* sex-linked mitochondrial DNAs (Bivalvia Mytilidae). BMC Genom. 12, 19. https://doi.org/10.1186/1471-2164-12-442.
Pettibone, M.H., 1984. A new scale-worm commensal with deep-sea mussels on the Galapagos hydrothermal vent (Polychaeta: polynoidae). Proc. Biol. Soc. Wash. 97, 226–239.
Plouviez, S., Shank, T.M., Faure, B., Daguin-Thiebaut, C., Viard, F., Lallier, F.H., Jollivet, D., 2009. Comparative phylogeography among hydrothermal vent species along the East Pacific Rise reveals vicariant processes and population expansion in the South. Mol. Ecol. 18, 3903–3917. https://doi.org/10.1111/j.1365-294X.2009.04325.x.
Rambaut, A., Drummond, A.J., Xie, D., Baele, G., Suchard, M.A., 2018. Posterior summarization in Bayesian phylogenetics using Tracer 1.7. Syst. Biol. 67, 901–904. https://doi.org/10.1093/sysbio/syy032.
Ronquist, F., Teslenko, M., van der Mark, P., Ayres, D., Darling, A., Hohna, S., Larget, B., Liu, L., Suchard, M., Huelsenbeck, J., 2012. Efficient Bayesian phylogenetic inference and model choice across a large model space. Syst. Biol. 61, 539–542.
Saether, K.P., Little, C.T.S., Campbell, K.A., Marshall, B.A., Collins, M., Alfaro, A.C., 2010. New fossil mussels (Bivalvia: Mytilidae) from Miocene hydrocarbon. Zootaxa 2577, 1–45.
Sahling, H., Masson, D.G., Ranero, C.R., Hühnerbach, V., Weinrebe, W., Klaucke, I., Bürk, D., Brückmann, W., Suess, E., 2008. Fluid seepage at the continental margin offshore Costa Rica and southern Nicaragua. G-cubed 9, Q05S05. https://doi.org/10.1029/2008GC001978.
Samadi, S., Puillandre, N., Pante, E., Boisselier, M.-C., Corbari, L., Chen, W.J., Maestrati, P., Mana, R., Thubaut, J., Zuccon, D., Hourdez, S., 2015. Patchiness of deep-sea communities in Papua New Guinea and potential susceptibility to anthropogenic disturbances illustrated by seep organisms. Mar. Ecol. 36, 109–132. https://doi.org/10.1111/maec.12204.
Sellanes, J., Quiroga, E., Neira, C., 2008. Megafauna community structure and trophic relationships at the recently discovered Concepción Methane Seep Area, Chile, ~36°S. ICES J. Mar. Sci. 65, 1102–1111. https://doi.org/10.1093/icesjms/fsn099.
Shimodaira, H., 2002. An approximately unbiased test of phylogenetic tree selection. Syst. Biol. 51, 492–508. https://doi.org/10.1080/10635150290069913.
Smith, P.J., McVeagh, S.M., Won, Y., Vrijenhoek, R.C., 2004. Genetic heterogeneity among New Zealand species of hydrothermal vent mussels (Mytilidae: Bathymodiolus). Mar. Biol. 144, 537–545. https://doi.org/10.1007/s00227-003-1207-4.
Solis-Weiss, V., Hernandez-Alcantara, P., 1994. *Amphisamytha fauchaldi*: a new species of Ampharetid (Annelida: polychaeta) from the hydrothermal vents at Guaymas Basin, Mexico. Bull. South Calif. Acad. Sci. 93, 127–134.
Stamatakis, A., 2014. RAxML version 8: a tool for phylogenetic analysis and post-analysis of large phylogenies. Bioinformatics 30, 1312–1313. https://doi.org/10.1093/bioinformatics/btu033.
Stiller, J., Rousset, V., Pleijel, F., Chevaldonné, P., Vrijenhoek, R.C., Rouse, G.W., 2013. Phylogeny, biogeography and systematics of hydrothermal vent and methane seep *Amphisamytha* (Ampharetidae, Annelida), with descriptions of three new species. Syst. Biodivers. 11, 35–65. https://doi.org/10.1080/14772000.2013.772925.
Swofford, D.L., 2002. Phylogenetic Analysis Using Parsimony (*and Other Methods), fourth ed. Sinauer Associates, Inc, Sunderland, MA.
Tang, Y., Horikoshi, M., Li, W., 2016. ggfortify: unified interface to visualize statistical result of popular R packages. R J 8.
Taylor, J.D., Glover, E.A., 2010. Chemosymbiotic bivalves. In: Kiel, S. (Ed.), The Vent and Seep Biota: Aspects from Microbes to Ecosystems. Springer. https://doi.org/10.1007/978-90-481-9572-5.
Thubaut, J., Puillandre, N., Faure, B., Cruaud, C., Samadi, S., 2013. The contrasted evolutionary fates of deep-sea chemosynthetic mussels (Bivalvia, Bathymodiolinae). Ecol. Evol. 3, 4748–4766. https://doi.org/10.1002/ece3.749.
Van Dover, C.L., Humphris, S.E., Fornari, D., Cavanaugh, C.M., Collier, R., Goffredi, S.K., Hashimoto, J., Lilley, M.D., Reysenbach, A.L., Shank, T.M., Von Damm, K.L., Banta, A., Gallant, R.M., Gotz, D., Green, D., Hall, J., Harmer, T.L., Hurtado, L.A., Johnson, P., McKiness, Z.P., Meredith, C., Olson, E., Pan, I.L., Turnipseed, M., Won, Y., Young III, C.R., Vrijenhoek, R.C., 2001. Biogeography and ecological setting of Indian Ocean hydrothermal vents. Science 294, 818–823. https://doi.org/10.1126/science.1064574.
Vrijenhoek, R.C., 2010. Genetic diversity and connectivity of deep-sea hydrothermal vent metapopulations. Mol. Ecol. 19, 4391–4411. https://doi.org/10.1111/j.1365-294X.2010.04789.x.
Whiting, Michael F., Carpenter, James C., Wheeler, Quentin D., Wheeler, Ward C., 1997. The Strepsiptera problem: Phylogeny of the holometabolous insect orders inferred from 18S and 28S ribosomal DNA sequences and morphology. Syst. Biol. 46 (1), 1–68. https://doi.org/10.2307/2413635.
Wickham, H., 2016. ggplot2: Elegant Graphics for Data Analysis. Springer-Verlag, New York.
Won, Y., Young, C.R., Lutz, R.A., Vrijenhoek, R.C., 2003. Dispersal barriers and isolation among deep-sea mussel populations (Mytilidae: *Bathymodiolus*) from eastern Pacific hydrothermal vents. Mol. Ecol. 12, 169–184. https://doi.org/10.1046/j.1365-294X.2003.01726.x.
Xu, T., Feng, D., Tao, J., Qiu, J.-W., 2019. A new species of deep-sea mussel (Bivalvia: Mytilidae: *Gigantidas*) from the South China Sea: morphology, phylogenetic position, and gill-associated microbes. Deep. Res. Part I Oceanogr. Res. Pap. 146, 79–90. https://doi.org/10.1016/j.dsr.2019.03.001.
Zapata-Hernández, G., Sellanes, J., Thurber, A.R., Levin, L.A., 2014. Trophic structure of the bathyal benthos at an area with evidence of methane seep activity off southern Chile (~45°S). J. Mar. Biol. Assoc. U. K. 94, 659–669. https://doi.org/10.1017/S0025315413001914.
Zouros, E., Ball, A.O., Saavedra, C., Freeman, K.R., 1994. An unusual type of mitochondrial DNA inheritance in the blue mussel *Mytilus*. Proc. Natl. Acad. Sci. U.S. A. 91, 7463–7467. https://doi.org/10.1073/pnas.91.16.7463.